THE PENNSYLVANIA STATE UNIVERSITY
SCHREYER HONORS COLLEGE

DEPARTMENT OF MECHANICAL AND NUCLEAR ENGINEERING

REFINEMENT OF HANDHELD SLIP RESISTANCE TRIBOMETER

NICHOLAS NACE
SPRING 2018

A thesis
submitted in partial fulfillment
of the requirements
for baccalaureate degrees
in Mechanical and Nuclear Engineering
with honors in Mechanical Engineering

Reviewed and approved* by the following:

H. J. Sommer III
Professor of Mechanical and Nuclear Engineering
Thesis Supervisor

Sean Brennan
Professor of Mechanical and Nuclear Engineering
Honors Adviser

* Signatures are on file in the Schreyer Honors College.

ABSTRACT

The designs of current tribometers used to test walkway surfaces are overly complex and result in high testing costs for customers. Stauffer's research validated the function of a new, simpler tribometer prototype that operates using strain gauges. Stauffer's handheld tribometer design was validated, but was not ergonomic, aesthetic, or manufacturable. A refined handheld tribometer design was designed and the hardware was fabricated by incorporating new technology and focusing on the missing attributes listed above.

TABLE OF CONTENTS

LIST OF FIGURES iv

LIST OF TABLES vii

ACKNOWLEDGEMENTS viii

Chapter 1 Literature Review 1

1.1 Need for Slip-Resistance Measurement and a New Measuring Device 1
1.2 National Flooring Safety Institute Approved Tribometers 3
1.3 Handheld Tribometers 8
1.4 Dual Beam Friction Pad Prototype 11

Chapter 2 Refinement of the Dual Beam Friction Pad 17

2.1 Design Approach 17
2.2 Redesign of Shoe and Square 19
2.2.1 Issues with the Prototype 19
2.2.2 Concept Generation and Selection 20
2.2.3 Detailed Design 22
2.3 Refinement of Pivot Block and Beam 27
2.3.1 Issues with Prototype 27
2.3.2. Refined Designs 27
2.4 Redesign of Electronics Enclosure and Handle 33
2.4.1 Issues with Prototype 33
2.4.2 New Designs 33
2.5 Electronics 39
2.5.1 Strain Gauges 39
2.5.2 Microprocessor 41

Chapter 3 Refined Handheld Tribometer Assembly 43

3.1 Hardware 43
3.2 Electronics 52

Chapter 4 Standards for Testing 55

4.1 American National Standards Institute Terminology 55
4.2 Test Procedures 55

Chapter 5 Recommendations for Future Work 59

5.1 Problems Encountered and Lessons Learned 59

5.2 Recommendations for Next Iterations.....60
5.3 Design for Specific Applications 61

BIBLIOGRAPHY.....62

APPENDIX A SolidWorks Drawings of Fabricated Parts.....64

APPENDIX B Bill of Materials.....72

LIST OF FIGURES

Figure 1: GMG-200 Tribometer [8] 4

Figure 2: GMG-200 and Anchoring Plate Setup Prior to Surface Testing [8] 4

Figure 3: Universal Walkway Tester Binary Output Tribometer 3000E [9] 5

Figure 4: Gold Standard 1 Tribometer with Sample Display of SCOF Test Results [10] 6

Figure 5: TRACSCAN tribometer with components and accessories [11] 7

Figure 6: H94 Handheld Tribometer [12] 9

Figure 7: H37 3D Portable Handheld Friction Tester [12] 10

Figure 8: Labeled Image of Main Mechanical Components in the DBFP [7] 12

Figure 9: Beam Deflections from Horizontal and Vertical Forces [7] 13

Figure 10: Underside of DBFP Highlighting the Locations of the Strain Gauges [7] 13

Figure 11: Block Diagram for DBFP Circuit [7] 14

Figure 12: Circuit Schematic for DBFP [7] 15

Figure 13: Flow Chart for DBFP [7] 16

Figure 14: Future Recommendation for DBFP Handle and Electronics Enclosure [7] 17

Figure 15: Tribometer System Breakdown 19

Figure 16: SolidWorks Part of Shoe 24

Figure 17: SolidWorks Part of Mounting Piece 24

Figure 18: Tipping Diagram for DBFP [7] 25

Figure 19: Preliminary Assembly of Shoe, Mounting Piece, and Neolite Pad 26

Figure 20: View of Right Face of Assembly Showing Height of Preliminary Assembly 26

Figure 21: SolidWorks Part of Beam 29

Figure 22: SolidWorks Assembly of Pivot Block with Shoulder Bolts and Bearings 29

Figure 23: Isometric View of Assembled Shoe, Mounting Piece, Beam, and Pivot Block 30

Figure 24: Right View of Assembly Shown in Figure 19 with Pivot Point Height Label 31

Figure 25: Stress Plot Generated from Static Study for Stainless Steel Beam Setup 32

Figure 26: Magpul MOE Pistol Grip [13].....34

Figure 27: Polycase Potting Box Enclosure and Lid 35

Figure 28: Cross Section of How Grip Connects to Rifle.....36

Figure 29: Isometric View of Wedge.....37

Figure 30: One of Two Arms that Connect the Electronics Enclosure to the Base 38

Figure 31: Preliminary Assembly of Electronics Enclosure (Lid Excluded).....38

Figure 32: Full Bridge Strain Gauge Designed for Small, Double-Bending Beam [14] 39

Figure 33: Full Bridge Strain Gauge for Single Surface Gauging of Transducers [14].....40

Figure 34: Simplified Circuit Schematic 41

Figure 35: SolidWorks Subassembly of Neolite, Shoe, and Mount 44

Figure 36: SolidWorks Subassembly of Pivot Block and Beam.....45

Figure 37: SolidWorks Subassembly of Arm and Bearing.....45

Figure 38: SolidWorks Subassembly of Case, Grip, and Wedge 46

Figure 39: SolidWorks Assembly of Tribometer Handle 47

Figure 40: SolidWorks Assembly of Tribometer Base.....48

Figure 41: SolidWorks Assembly of Tribometer (No Electronics) 49

Figure 42: Isometric View of Physical Assembly 49

Figure 43: Top View of Physical Assembly 50

Figure 44: Front View of Physical Assembly.....50

Figure 45: Right View of Physical Assembly.....51

Figure 46: Beam with Two Full Bridges Installed and an Unsuccessful Soldering Attempt ..53

Figure 47: Close-up of Gauge with Solder Issues that Highlights Evidence of Error 53

Figure 48: Setup of Bridge Wired to Strain Indictor to Display Strain Readings.....54

Figure 49: Polycase Diecast Aluminum Enclosures 60

Figure 50: SolidWorks Drawing of Shoe....64
Figure 51: SolidWorks Drawing of Mount....65
Figure 52: SolidWorks Drawing of Beam....66
Figure 53: SolidWorks Drawing of Pivot Block....67
Figure 54: SolidWorks Drawing of Arm....68
Figure 55: SolidWorks Drawing of Enclosure....69
Figure 56: SolidWorks Drawing of Wedge....70
Figure 57: SolidWorks Drawing of Washers....71

LIST OF TABLES

Table 1: Summary of NFSI Approved Tribometers [6], [8], [9], [10], [11] 7

Table 2: AHP Matrix for Shoe and Mounting Piece Criteria.....21

Table 3: Scoring Matrix for Shoe and Mounting Piece Concepts.....22

Table 4: Bill of Materials.....72

ACKNOWLEDGEMENTS

I would like to thank Dr. Sommer for presenting the opportunity to pursue this thesis under his guidance, as well as equipping me with quality skills in machine design I learned both in and out of the classroom. I would also like to thank Dr. Brennan for reviewing my thesis, as well as guiding me through my undergraduate education as my advisor and enhancing my understanding of mechatronics as my professor. I would also like to thank Dr. Coyle for taking the time to introduce me to strain gauge experiments in my first honors class that helped prepare me to be a Schreyer Scholar. Lastly, I would like to thank my mom for being there for me my whole life. From when you would rock me to sleep in my crib as an infant, stay up late helping me with my homework in elementary school, and even up to the end of my undergraduate career when you would call to check in on me, you were always there. I would not be the person I am today without your support.

Chapter 1

Literature Review

1.1 Need for Slip-Resistance Measurement and a New Measuring Device

The need for better procedures, equipment, work environments, and standards are crucial to reduce mortality and injury rates related to slips, trips, and falls (STF). According to the Bureau of Labor Statistics, STF were the second highest leading cause of occupational fatalities in 2015, as well as the second leading cause of missed days at work [1], [2]. Accompanying these tragedies are monetary losses that amount to over $30 billion in direct expenses every year [3]. In 2015, medical costs for falls totaled more than $50 billion [4]. Outside of the occupational injuries, the risk of injury or death for seniors past the age of 65 from a slip or fall increases along with the associated medical bills [3]. With a growing population and the generation of baby boomers in the senior stage of their lifetime, STF incidents are occurring more frequently every year.

In regulating walkway surfaces, friction, or slip resistance, of surfaces are assessed using tribometers. There are many different tribometers used to assess surfaces, and the test results of many tribometers can be inconsistent [5]. The American National Standards Institute (ANSI) sets standards for walkways surfaces and walkway surface testing, but the National Flooring Safety Institute (NFSI) is an organization that has a stronger focus on walkway regulations and contributes to the development of standards that ANSI publishes. To reduce the deviation of

testing results across tribometer models, NFSI requires that tribometer manufacturers submit an inter-laboratory study that proves the testing capabilities of the tribometer are reproducible [6]. Among the many tribometers available for use, the NFSI has approved only four tribometers for friction testing in validating walkway surface safety [6].

Although a limited number of possible designs that can be used to test surfaces helps with standardization, NFSI approved tribometers are arguably oversized and overdesigned, resulting in high costs for the consumer. The lack of variety among the expensive designs, in combination with old technology, creates an opportunity to design a handheld tribometer using new technology and design for manufacturability (DFM) techniques. A tribometer that is more easily manufactured could make walkway surface testing more affordable for the consumer, as well as increase the accessibility to surface testing options. That is, purchasing a readily available inexpensive tribometer is more feasible than renting an expensive tribometer.

Jonah Stauffer pursued this “new design” in 2001, initiating the design of a handheld tribometer [7]. While Stauffer validated the function of his tribometer, the ergonomic, aesthetic, and manufacturability aspects of the handheld tribometer design were not the focus of his research. Refinement of Stauffer’s design will advance tribometer technology and change the friction measuring industry to be more customer friendly.

1.2 National Flooring Safety Institute Approved Tribometers

NFSI is the institute responsible for overseeing a specific committee on STF prevention, as well as providing product testing and certification, educational training, and standards development for the flooring industry [6]. When testing walkway surfaces, only NFSI approved tribometers should be used. NFSI approves each tribometer for static coefficient of friction (SCOF) testing, dynamic coefficient of friction (DCOF) testing, or both.

The first NFSI approved tribometer is the GMG-200, manufactured by the German company GTE Industrieelektronik [6], [8]. The GMG-200 tribometer is only approved for DCOF measurement [6]. The GMG-200 operates by dragging itself along a surface, using a motor to wind a cable that is anchored to the ground by the user's foot [8]. As the GMG-200 drags along the surface, the device uses the force required to overcome the friction force opposing the movement to compute a DCOF for the surface [8]. The test is repeated to ensure the readings are consistent and there are no problems with the tribometer, and the results of each trial are displayed on a LCD. The test results can be printed or downloaded from the GMG-200. The GMG-200 tribometer and test setup can be seen in Figure 1 and Figure 2, respectively.

Figure 1: GMG-200 Tribometer [8]

Figure 2: GMG-200 and Anchoring Plate Setup Prior to Surface Testing [8]

The second NFSI approved tribometer is the Universal Walkway Tester (UWT) [6]. The latest model of the UWT is the Binary Output Tribometer (BOT) 3000E, manufactured by Regan Scientific Instruments [9]. While the BOT-3000E is capable of testing both SCOF and DCOF, NFSI only approves this tribometer for SCOF testing [6]. The BOT-3000E operates similarly to the GMG-200 tribometer in that it drags itself along a surface and uses motor forces to compute a COF, but an anchor is not required. The user must select desired tests using a display screen and follow instructions during tests, such as rotating the tribometer 90 or 180 degrees after a run.

When a test is completed, a report of the tests can be printed or downloaded from the USB port on the BOT and serve as documentation that the given surface passed walkway tests [9]. The data on the report includes photos of the test surface taken by the BOT during testing, graphs of the DCOF reading over the distance the test was conducted (if applicable), temperature and humidity readings, average COF for all of the runs, and the date and time the test was done [9]. Figure 3 shows the BOT-3000E.

Figure 3: Universal Walkway Tester Binary Output Tribometer 3000E [9]

The third NFSI approved tribometer is the Gold Standard (GS) 1 [6]. The GS-1 tribometer is NFSI approved for both SCOF and DCOF testing, manufactured by Johnson Forensic Lab, and distributed by Impact General, Inc. [6], [10]. The GS-1 operates similarly to the BOT-3000E and GMG-200 in that it drags a weight across a surface and measures the horizontal force required to move the weight. A COF is calculated based on the forces required to move the weight [10]. The distinguishing characteristic of the GS-1 is the separate weight that the tribometer drags behind itself, rather than having the weight be a part of the hardware assembly, shown in Figure 4.

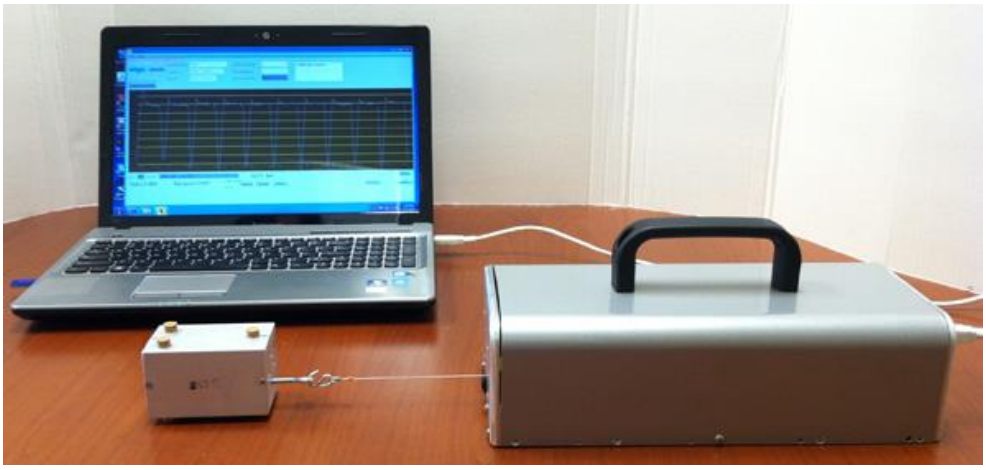

Figure 4: Gold Standard 1 Tribometer with Sample Display of SCOF Test Results [10]

The last of the NFSI approved tribometers is the TRACSCAN tribometer. The TRACSCAN is NFSI approved for SCOF and DCOF measurement and is manufactured and distributed by MAD Safety Instruments [6], [11]. The history of the TRACSCAN tribometer can be traced back to a German company that designed the robotic tribometer that the BOT-3000 tribometer was modeled after, so the designs of the TRACSCAN and BOT-3000E tribometers are nearly identical [11]. In fact, the only differences that could be found were the appearance and potentially minor differences in display menu options. In terms of similarity, the TRACSCAN tribometer tests surfaces the same way as the BOT-3000E, as well as generates a report that can be downloaded or printed from the device [11]. The TRACSCAN tribometer, as well as some items required for storage, charging, and data retrieval, are shown in Figure 5.

Figure 5: TRACSCAN tribometer with components and accessories [11]

Summarizing the NFSI approved tribometers, each tribometer has a "box-like" design that is dragged along a surface and records test results that can be printed and downloaded from the tribometer. Each design calculates a COF within the range of zero to one. In other words, none of the tribometers measure adhesion. Lastly, all of the tribometers are available to consumers for around $7,000. Table 1 summarizes some of the qualities of each tribometer relevant to this research.

Table 1: Summary of NFSI Approved Tribometers [6], [8], [9], [10], [11]

Tribometer Model	SCOF Testing Approved	DCOF Testing Approved	Size[a] (L×W×H; in.)	Weight (lb)	Cost[b] ($)
GMG-200		✓	6.5 × 8.0 × 6.0	20	N/A*
UWT BOT-3000E	✓		11.5 × 7.0 × 4.5	17	7,000
GS-1	✓	✓	12.5 × 5.5 × 5.5	7.3	7,500
TRACSCAN	✓	✓	N/A**	N/A**	7,000

[a]Size is rounded to nearest half inch.
[b]Cost rounded to nearest $500.
*GMG-200 manufacturer is based in Germany, so use of this tribometer in America is scarce due to large shipping costs and availability of other options.
**Exact dimensions and weigh were not listed, but dimensions are similar to that of BOT-3000E.

1.3 Handheld Tribometers

While there are no more NFSI approved tribometers outside of those discussed in Section 1.2, some handheld tribometers have been designed since Stauffer's research. For the sake of addressing the only handheld tribometers on the market and assuring Stauffer's handheld design is not at risk of copyright infringement, two tribometer designs from the company Kett are briefly discussed.

The first of Kett's tribometers is the H94 Handheld Tribometer. This tribometer operates using a voice coil motor fixed onto a slider and a photo sensor [12]. When the slider begins to move, a microprocessor takes the force vectors and uses them to compute a coefficient of friction [12]. The tribometer outputs the result on the display. The H94 Handheld Tribometer only measures SCOF. The H94 Handheld Tribometer is much more compact than the NFSI approved tribometers, as shown in Figure 6.

Figure 6: H94 Handheld Tribometer [12]

The other handheld tribometer Kett offers is the H37 3D Portable Handheld Friction Tester. The H37 3D Portable Handheld Friction Tester also operates using a voice coil motor and a photo sensor, similar to the H94 Handheld Tribometer [12]. The difference between the H37 and H94 models is that the H37 tribometer can be held against a non-horizontal surface and perform the same function as the H94 tribometer [12]. The H37 tribometer also only measures SCOF [12]. The H37 3D Portable Handheld Friction Tester is similar in size and weight to the H94 Handheld Tribometer, but it has a more ergonomic handle that allows the user to test non-horizontal surfaces, as shown in Figure 7.

Figure 7: H37 3D Portable Handheld Friction Tester [12]

The handheld tribometers that Kett offers are able to measure friction to the accuracy of one one-thousandth, and even measure COF greater than one [12]. This resolution and extended range of measurement implies that these tribometers are designed more for thin film research than they are for walkway surface testing. While Kett did manage to develop the first handheld tribometer, the designs do not pose serious competition to Stauffer's design due to being designed for a field outside of walkway safety, along with operating with the use of motors like the NFSI approved tribometers. The handheld design Stauffer proposed does not operate using motors, which will be discussed in Section 1.4.

1.4 Dual Beam Friction Pad Prototype

All of the NFSI approved and handheld tribometers operate using motors that measure forces required to overcome friction. The tribometer Stauffer designed operates by a user moving the tribometer along a surface, causing two beams of the tribometer to get loaded differentially [7]. Strain gauges measure resultant strain in the beams, and a microprocessor uses the strain readings to compute a COF for a surface [7]. Stauffer's design eliminated the need for a motor, which resulted in a much more simplified tribometer design than those of available tribometers on the market.

The handheld dual beam friction pad (DBFP) tribometer Stauffer designed can be broken down into two primary systems – the mechanical system that is responsible for structural integrity and deformation in response to testing, and the electrical system that measures beam deflection and computes a COF corresponding to the strain readings [7]. The hardware that makes up the mechanical aspect of the DBFP includes a square, yoke pivot block, pivot, handle, shoe, and beams, as shown in Figure 8 [7].

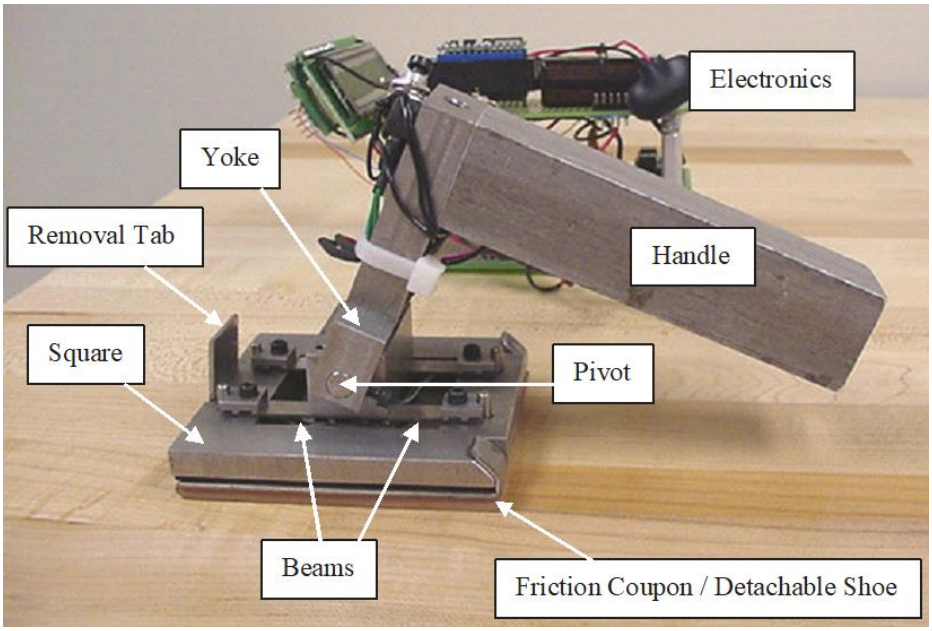

Figure 8: Labeled Image of Main Mechanical Components in the DBFP [7]

When the device is used, the beams will deflect in a manner similar to that shown in Figure 9. Figure 9 shows the beam deflection in two scenarios – purely horizontal force response and purely vertical force response. During operation, however, both horizontal and vertical forces will be exerted on the device, resulting in asymmetrical deformation between the leading and trailing beams, which will allow two unique strains to be read by the strain gauges [7].

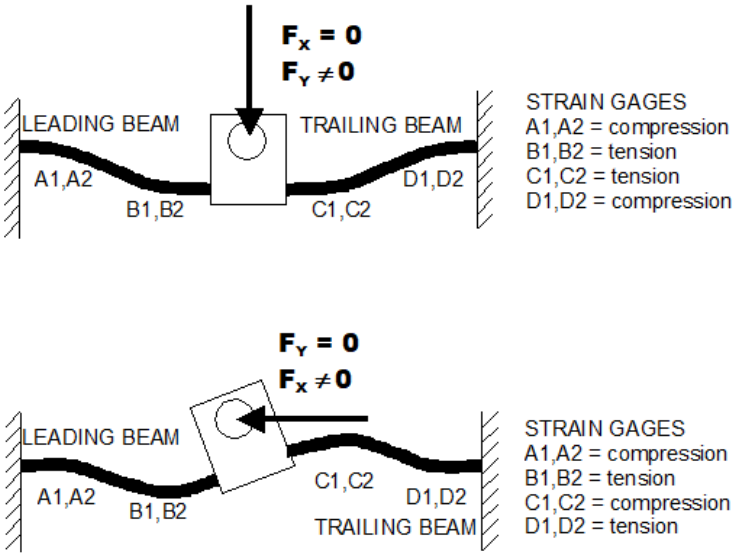

Figure 9: Beam Deflections from Horizontal and Vertical Forces [7]

In Figure 10, the strain gauge locations are shown on the bottoms of the beams, with the leading beam gauges at the front of the tribometer (removal tab side) and the trailing beam gauges in the rear of the tribometer (handle side) [7].

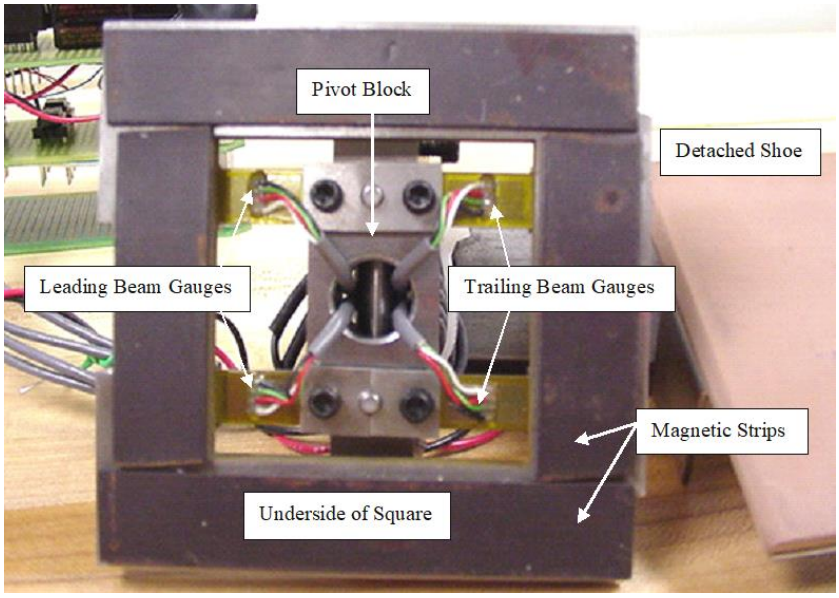

Figure 10: Underside of DBFP Highlighting the Locations of the Strain Gauges [7]

The strain gauges are wired so a Wheatstone bridge is created for the front and rear sides of both beams, meaning four Wheatstone bridge circuits are used in the overall strain measurement [7]. When strain is measured, amplifiers receive and send the amplified signals to A/D converters and the microprocessor to compute COF [7]. Figure 11 and Figure 12 convey specific details of the circuitry using a block diagram and circuit schematic, respectively.

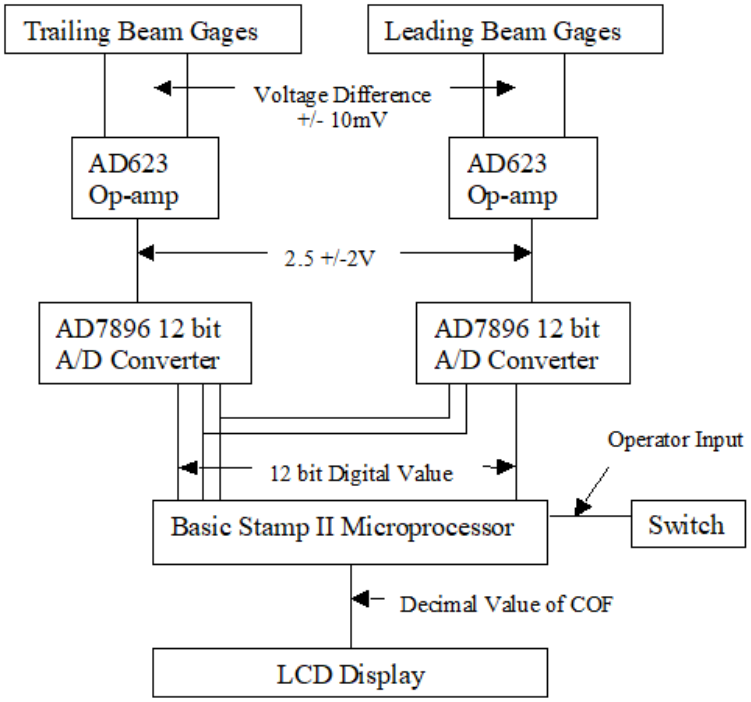

Figure 11: Block Diagram for DBFP Circuit [7]

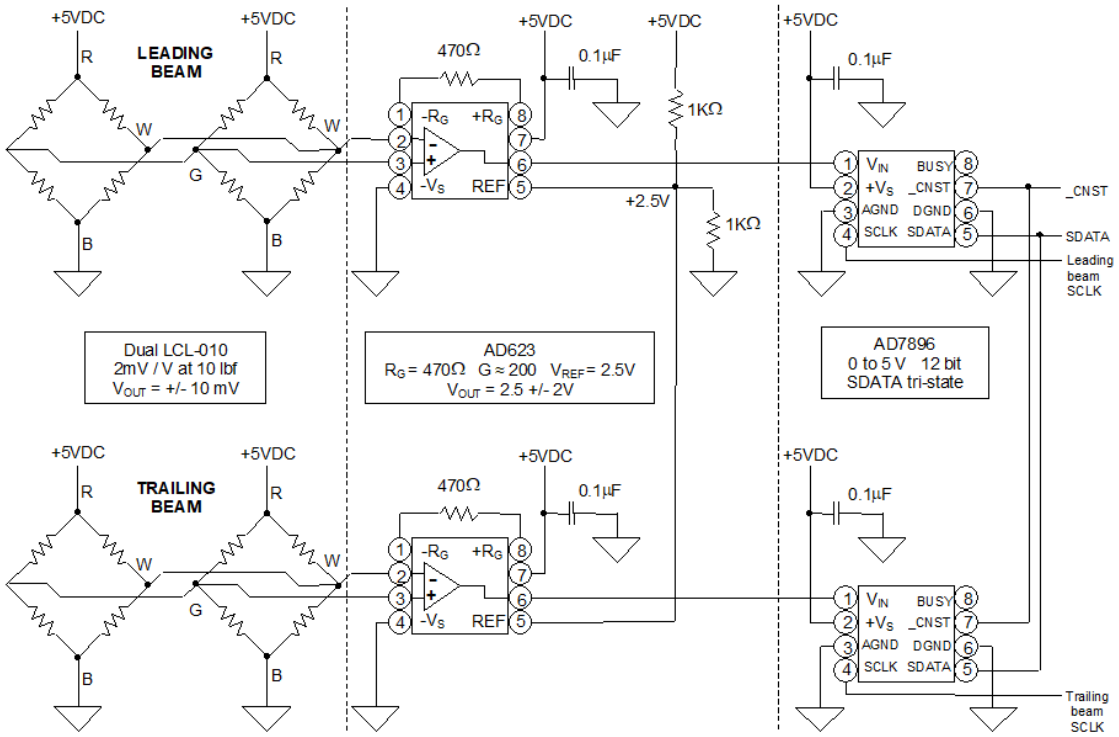

Figure 12: Circuit Schematic for DBFP [7]

The program for the DBFP was designed to store the data received during testing, as well as zero the strain gauges, eliminating error from thermal stresses and simply holding the tribometer. The flow chart for the DBFP program is shown in Figure 13.

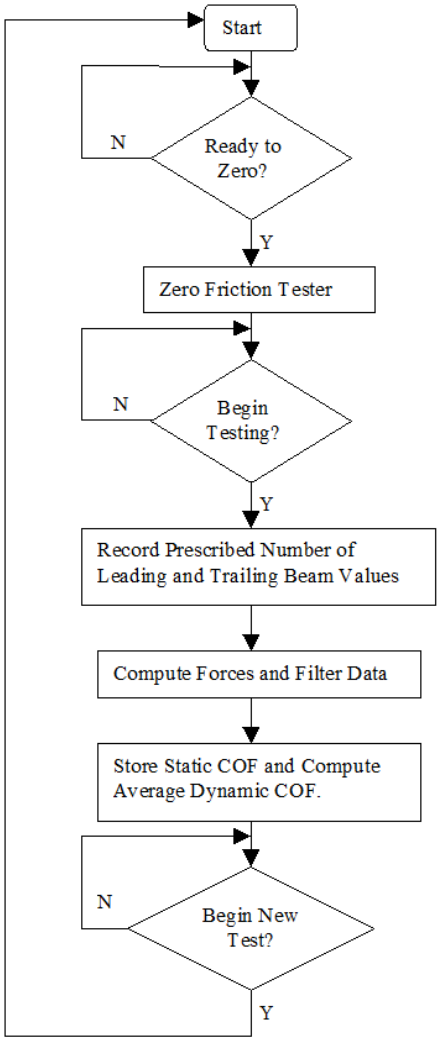

Figure 13: Flow Chart for DBFP [7]

Stauffer validated the DBFP functionality by comparing the results from a standard tile test to the results of a simple dragsled tribometer [7]. Stauffer found that the DBFP performs comparably with the dragsled tribometer, while noting that using the DBFP was less complicated to test than the dragsled, which required careful positioning due its dependence on gravity [7].

Chapter 2

Refinement of the Dual Beam Friction Pad

2.1 Design Approach

Stauffer focused on DBFP function. He managed to validate his tribometer design, but more work needs done to the DBFP if the design is going to reach industry standards. As shown in Figure 8, aesthetics and ergonomics clearly have room for improvement, and Stauffer noted this in his recommendations for future work [7]. Stauffer proposed a case to help contain some of the exposed electronics and wires, as shown in Figure 14 [7]. While the refined handle design does enhance the appearance of the tribometer, the new design hardly addressed the ergonomic issues with the DBFP.

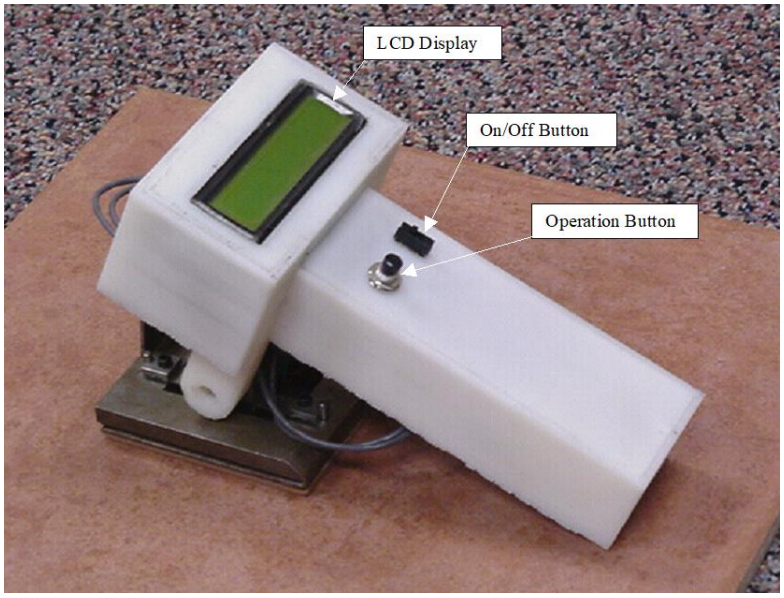

Figure 14: Future Recommendation for DBFP Handle and Electronics Enclosure [7]

Aside from the ergonomic and aesthetic aspects of the device, Stauffer did not design the DBFP for mass production. In other words, another area for improvement in design is manufacturability. Addressing the areas of ergonomics, aesthetics, and manufacturability requires changing the structure of the DBFP, which is integrated into the function of the device. That is, the strain in the beams is a function of some structural aspects of the DBFP, such as the dimensions of the beams and the size and location of the pivot block. If the structure of the DBFP changes, the microprocessor code that Stauffer used in the original design will need to be adjusted as well.

Along with the changes and recalibrations to the electronics that are required with any structural changes, technology that was unavailable during the design of the DBFP can be used in place of some components Stauffer had to use. For example, the use of external A/D converters is arguably unnecessary with new microcontrollers available today that can measure analog inputs.

Refinement of the DBFP in this thesis addresses the areas of ergonomics, aesthetics, and manufacturability. The refinement process ranged from simple modification to complete redesign of components. The design process proceeded from the bottom toward the top of the DBFP, starting with the shoe and square. This approach was taken in order to isolate subsystems in concept screening and testing processes, while causing minimal interaction with other subsystems that are dependent on the subsystems in that stage of the design / refinement process. The system breakdown in shown in Figure 15.

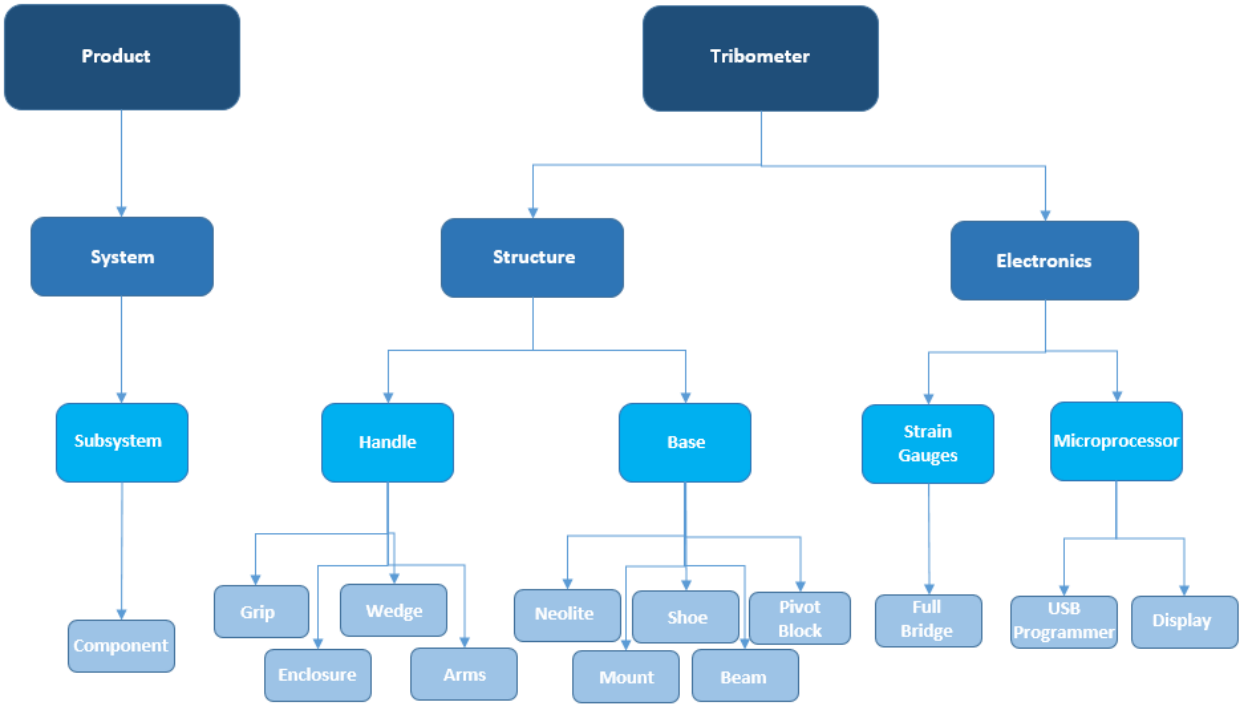

Figure 15: Tribometer System Breakdown

2.2 Redesign of Shoe and Square

2.2.1 Issues with the Prototype

The detachable shoe on the DBFP allows users to remove the shoe quickly, allowing for fast transition between testing coupons – the most common being a rubber called Neolite, but other rubbers are used as well. The detachable shoe works by hooking the rear end of the shoe around the back of the square and snapping the removal tab in place at the front of the square [7]. This process locks the shoe in place and magnets at the base of the square add additional force in keeping the shoe from moving - refer to Figure 8 and Figure 10 for aid in visualizing.

Stauffer's design allows for fast transition of testing materials, but the removal of the shoe requires a large force to be exerted on the removal tab. When the force exerted on the tab reaches the amount required to overcome the locking force, the shoe abruptly separates from the square. This process poses a small hazard for fingers. Accompanying this hazard are the pinch points that exist during the mating of the shoe and square. To address these hazards, the shoe and square were completely redesigned.

2.2.2 Concept Generation and Selection

Two options arose in generating ideas to replace the DBFP shoe. The first option was a round shoe, and the second was a square shoe. Because of how the shoe and square mate, the square was integrated in the redesign process with the shoe. Because the square is no longer guaranteed to be a square, the name of the component that serves as the square in the DBFP will be addressed as the mounting piece. The main challenges accompanying the redesign were determining how the shoe and mounting piece would lock together and how each component could be fabricated easily.

If the round shoe design were pursued, threading surfaces would be the most practical for interfacing the shoe and the mounting piece, as machining would be difficult to implement other options like bayonet or nut and bolt locks. If the square shoe were pursued, a larger variety of locking designs would be available to evaluate due to the flat edges of a square design, including options like holes that could interface with spring plungers and bolts. Another square shoe concept was generated when consideration was given to the structural integrity of the refined

design, ultimately breaking the square shoe option into two concepts. One concept would have the shoe made of sheet metal to wrap around the mounting piece, and the other concept would have the mounting piece made of sheet metal to fit around the shoe.

During ideation for redesign of the shoe and mounting piece, ease of assembly and fabrication were identified as the most important qualities. From these two qualities, more specific sub-categories were generated and used in an analytic hierarchy process (AHP) matrix to determine importance, as shown in Table 2. A scoring matrix then used the AHP matrix results to determine which concept was best to pursue. Table 3 shows the square concept with a shoe made of sheet metal to be the best option.

Table 2: AHP Matrix for Shoe and Mounting Piece Criteria

	Simplicity	**Ease of Fabrication**	**Structural Integrity**	**Cost**	**Row Total**	**Weight**
Simplicity	1.00	1.00	0.50	2.00	4.50	0.23
Ease of Fabrication	1.00	1.00	1.00	3.00	6.00	0.31
Structural Integrity	2.00	1.00	1.00	3.00	7.00	0.36
Cost	0.50	0.330	0.33	1.00	2.16	0.11
Total					19.67	1.00

Table 3: Scoring Matrix for Shoe and Mounting Piece Concepts

	Square Shoe and Mounting Piece; Sheet Metal Shoe		Square Shoe and Mounting Piece; Sheet Metal Mounting Piece		Round Shoe and Mounting Piece	
	Score	Weighted Score	Score	Weighted Score	Score	Weighted Score
Simplicity	5.00	1.14	5.00	1.14	3.00	0.69
Ease of Fabrication	4.00	1.22	5.00	1.53	2.00	0.61
Structural Integrity	5.00	1.78	2.00	0.71	5.00	1.78
Cost	4.00	0.44	4.00	0.44	2.00	0.22
Total Score	4.59		3.82		3.30	
Rank	1		2		3	

The main determining factor in the scoring matrix was the structural integrity criteria. While the two concepts for a square shoe and mounting piece were very similar, the load of the tribometer requires a sturdy foundation. If the mounting piece was made of sheet metal, the space left between the shoe and mounting piece (for wires and minor deflection) would focus too much stress on the thin material. However, the structural integrity of the mounting piece with a sheet metal shoe was not at risk of compromise due to a thick mounting piece that the sheet metal shoe could wrap around, resulting in only minor loads at bending points on the shoe.

2.2.3 Detailed Design

With the basic geometry of the shoe and mounting piece determined, focus was directed toward more specific aspects of the components, such as material composition, interfacing, and fabrication. Due to the shoe and mounting piece's lack of exposure to large stresses in structurally weak areas, aluminum was selected. The aluminum would not be susceptible to extreme deformation during operation, and it is the cheapest and most machinable material

available. For the sheet metal, 3003 aluminum is used for bending the material into the shoe shape (5000 and 6000 series do not bend well), while 6061 aluminum is used for the mounting piece. In fact, for these reasons, aluminum is the material of choice for all metal components in the refined tribometer design, with the important exception of the beam, which is explained later in this chapter.

Determining exact dimensions and interfacing was mostly done on the computer automated drafting (CAD) software SolidWorks. First, the exact dimensions were determined. The friction coupon material was available in 3 x 3 inch dimensions, so to keep design consistent and use as much of the material as possible, the shoe and mounting pieces were designed with three inch square dimensions. The height of the shoe and mounting pieces were made only large enough to house 10-24 screws that would mate the shoe and mounting pieces. This minimization of height is explained in detail later in this chapter. The CAD drawing for the shoe, mounting piece, and all of the remaining parts discussed can be found in Appendix A.

Because the shoe would be made from aluminum sheet metal, a sheet metal bending brake would be used to bend the sheet metal. The brake leaves a small radius where the sheet metal is bent, so if the shoe and mounting piece are to fit together, leading and trailing edges of the mounting piece must be chamfered to leave room for radii in the sheet metal bends. The final shoe and mounting piece designs are shown as SolidWorks Parts in Figure 16 and Figure 17. The additional holes in the mounting piece are for mating the beam to the mounting piece, which is discussed in Section 2.3.

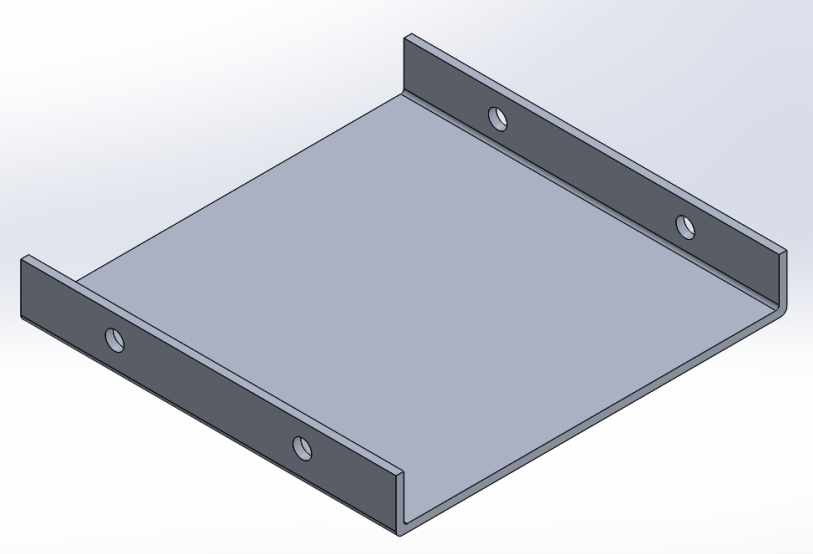

Figure 16: SolidWorks Part of Shoe

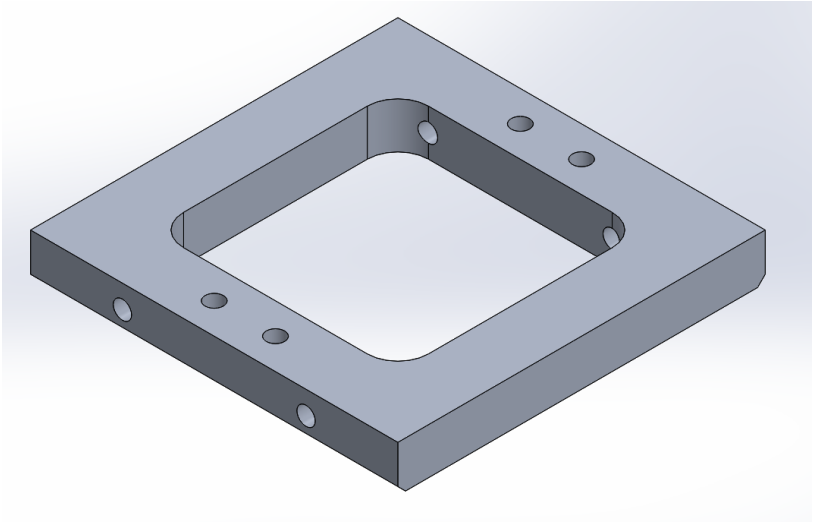

Figure 17: SolidWorks Part of Mounting Piece

The minimization in height was made not only for reducing required material, but also for leaving enough room to allow the pivot block to house components and prevent the device from tipping during operation. To prevent tipping, the height of the point of loading must be less than the distance between the center of pressure and from the horizontal position of the pivot point. This tipping diagram can be seen in Figure 18 for the DBFP.

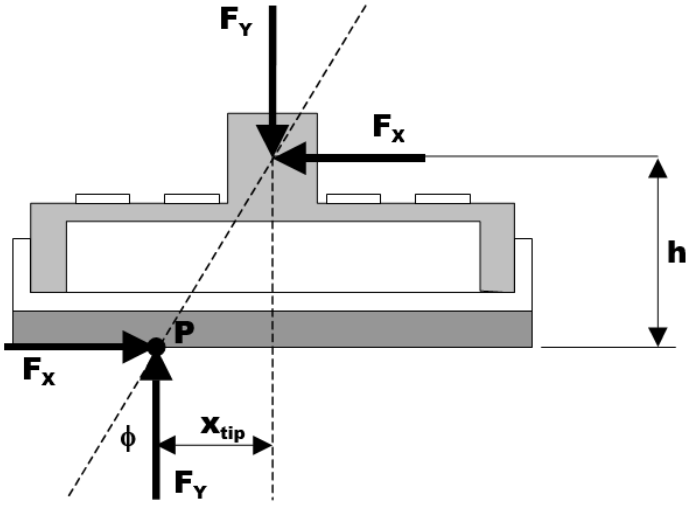

Figure 18: Tipping Diagram for DBFP [7]

Using trigonometry with the force vectors to solve for the COF, the following formula $\tan\phi = \mu$ is derived, where μ is the COF. Assuming the maximum COF that could be measured is $\mu_{max} = 1$, the maximum angle is $\phi_{max} = 45°$ and, consequently, the smallest possible distance between the center of pressure and the horizontal position of the pivot point is $x_{tip} = 1.5\ in$, given that the base of the tribometer is three inches long. Therefore, the height of the pivot point from the base of the tribometer (bottom of friction coupon where the surface contact occurs) must be less than one and one half inches.

With the current parts – shoes, mounting piece, and Neolite pad – the design is currently 0.5625 inches from the ground, leaving 0.9375 inches of space remaining for the pivot point. Figure 19 shows the isometric view of the current components, while Figure 20 shows the height of the preliminary assembly calculated by SolidWorks.

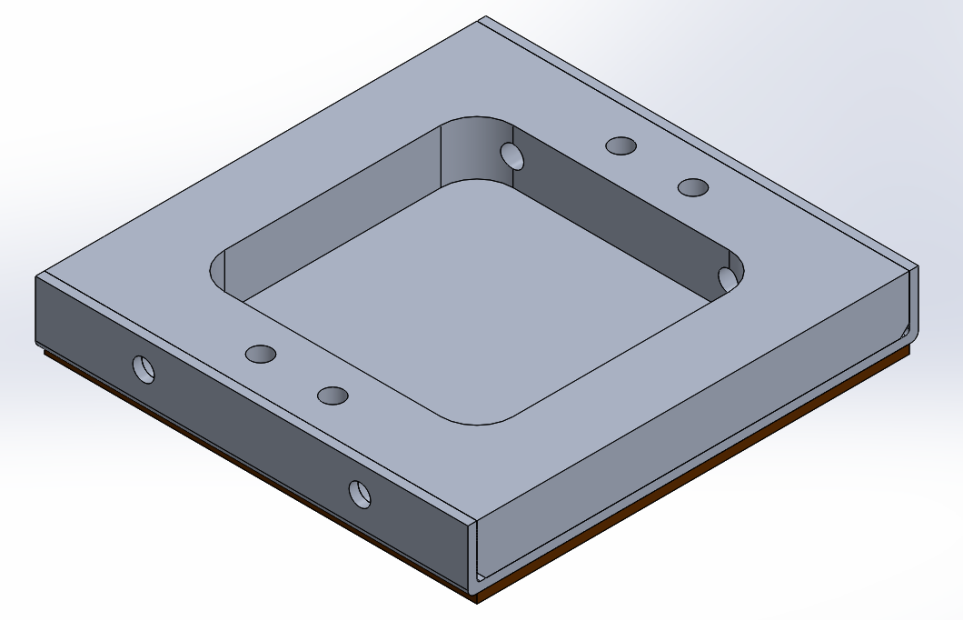

Figure 19: Preliminary Assembly of Shoe, Mounting Piece, and Neolite Pad

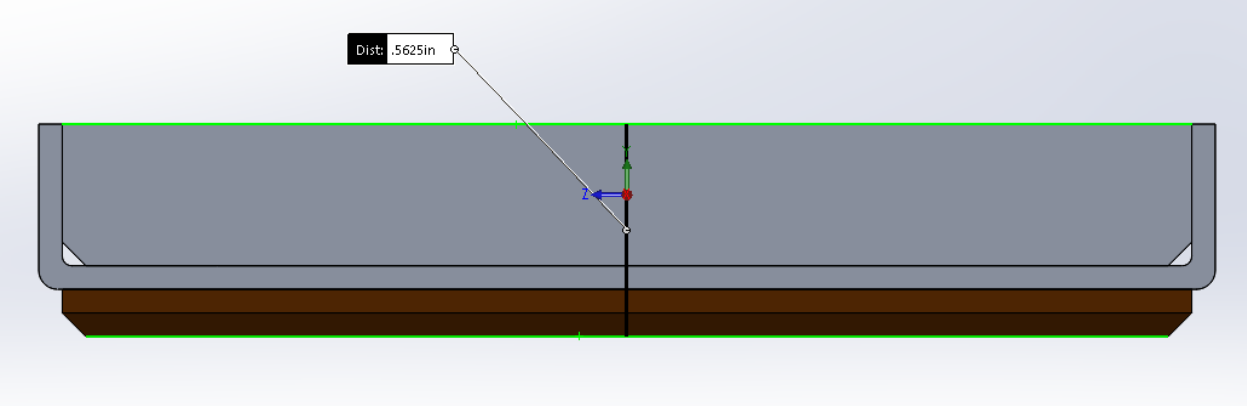

Figure 20: View of Right Face of Assembly Showing Height of Preliminary Assembly

2.3 Refinement of Pivot Block and Beam

2.3.1 Issues with Prototype

Stauffer's DBFP has four separate beams – the pivot block connects two pairs of beams that act as two separate beams. The small beams leave little room for any variability in strain gauge setup, which may be desired in future iterations of the design. The two beams also generate the same strain output, in theory, during operation, so some redundancy exists that can be eliminated to simplify the overall design.

Regarding the pivot block, a rod protrudes outside of the lateral edges of the pivot block to transfer force from the handle to the pivot block and, ultimately, the beams. Other than an interference fit, nothing is holding the rod in place. For a more secure structure, the rod can be replaced, modified, or contained by the handle so it will not fall out when in use or carried by a user.

2.3.2. Refined Designs

To simplify the complexity of the DBFP, the two narrow beams were replaced by one wide beam. This refined component eliminates the need for two of the four original Wheatstone bridges, reducing the complexity of the electronics and the structure of the DBFP, while maintaining the stability of two separate beams. The extra space also allows for more variability in taking strain measurements. That is, a Wheatstone bridge can be built using a variety of

premade strain gauges available for purchase and not be as limited with surface area to be able to assemble them.

With the refined beam design being wider, the pivot block becomes wider as well. This enlarged dimension increases the options for additional components to be used in mating the pivot block to the handle. The rod can now be replaced using shoulder bolts. The shoulder bolts are screwed into the pivot block, so there are threads holding the component in place instead of just an interference fit. When the shoulder bolt is completely inserted into the pivot block, a part of the shoulder bolt (the “shoulder”) is available to support the handle. The new design is securely fastened and maintains the original function of allowing the handle to pivot and transfer force to the beam. However, while having a plastic handle pivoting about a metal rod (shoulder) presents no issues, fabricating a custom plastic handle is not a cheap option. Therefore, assuming a plastic handle will not be pursued for future designs, bearings were incorporated into the pivot block to maintain a pivoting motion.

To connect the pivot block and beam, holes were drilled in the beam in locations suitable for screws to be inserted, as well as one hole in the center of the beam to allow wires to travel under and through the beam, through the pivot block, and finally to the electronics housing. The pivot block contains multiple holes for screws, shoulder bolts, and wires. Shown in Figure 21 and Figure 22 are the refined beam and pivot block designs, respectively. The pivot block is symmetrical, with all holes cut through the block.

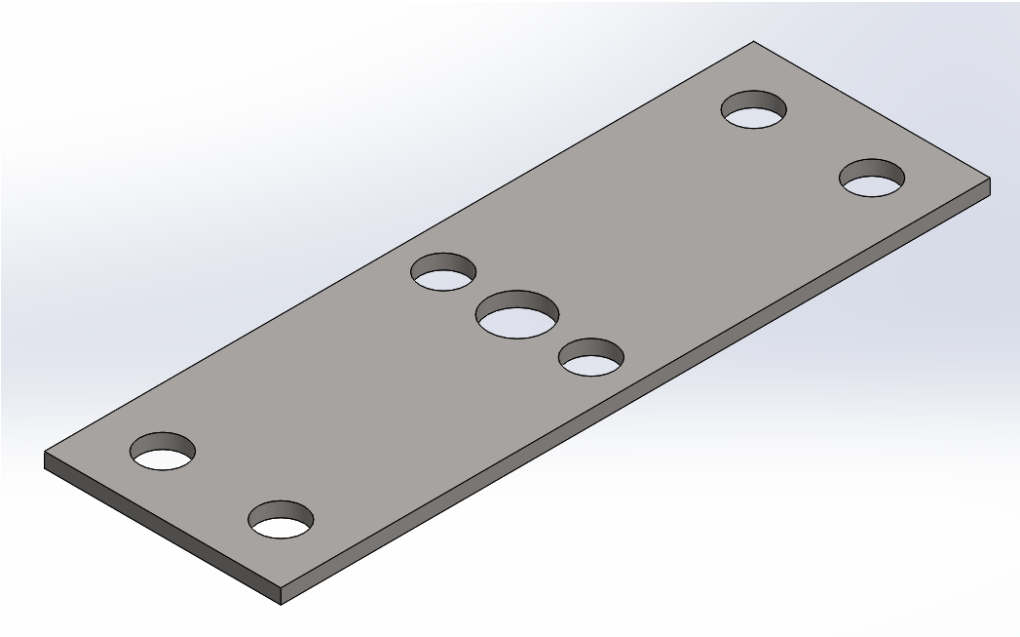

Figure 21: SolidWorks Part of Beam

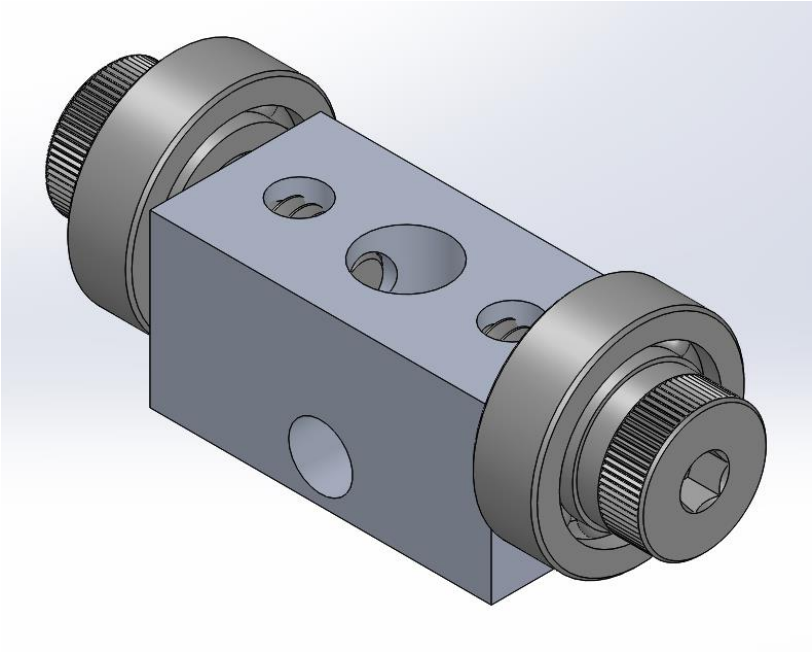

Figure 22: SolidWorks Assembly of Pivot Block with Shoulder Bolts and Bearings

Figure 22 displays a hole that is cut from the front surface of the pivot block to the rear face of the pivot block. This additional hole is for wires, just like the hole through the center of the block from the top to bottom faces. While no wires travel through this opening, this feature allows future designs to assemble strain gauges on the top of the beam and route the wires to the pivot block, rather than having them travel underneath the beam to the bottom hole in the pivot block. This feature allows for flexibility in strain gauge wiring for future iterations on the design.

Referring back to tipping mentioned in Section 2.2, the dimensions of the beam and pivot block were chosen with respect to keeping the pivot point less than one and one half inches from the bottom of the tribometer. Figure 23 and Figure 24 show the preliminary assembly of the components mentioned thus far from the isometric and right viewing planes, respectively, along with a label displaying the vertical distance of the pivot point to the bottom of the tribometer.

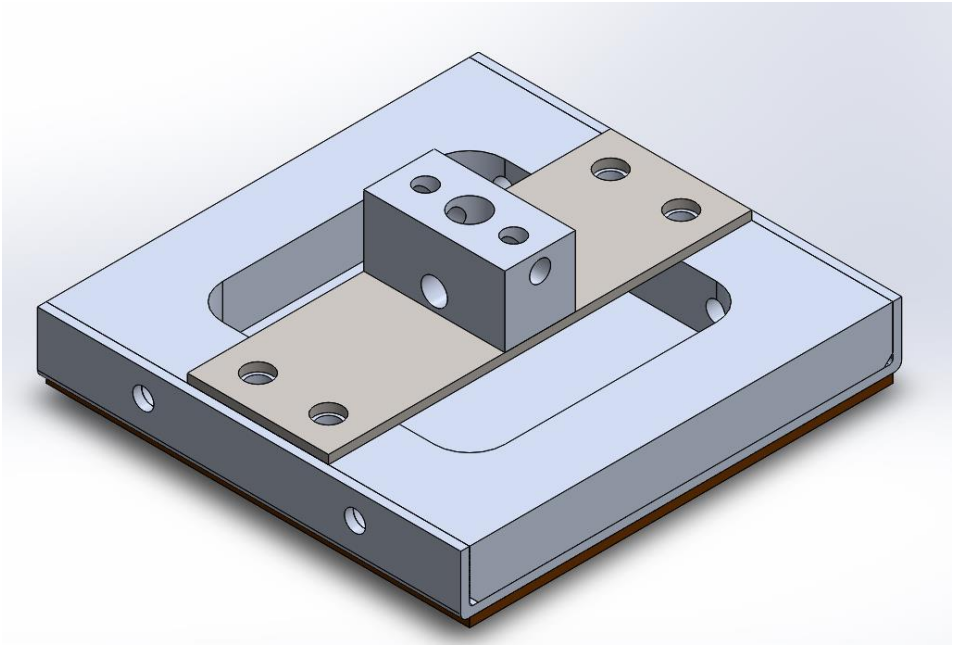

Figure 23: Isometric View of Assembled Shoe, Mounting Piece, Beam, and Pivot Block

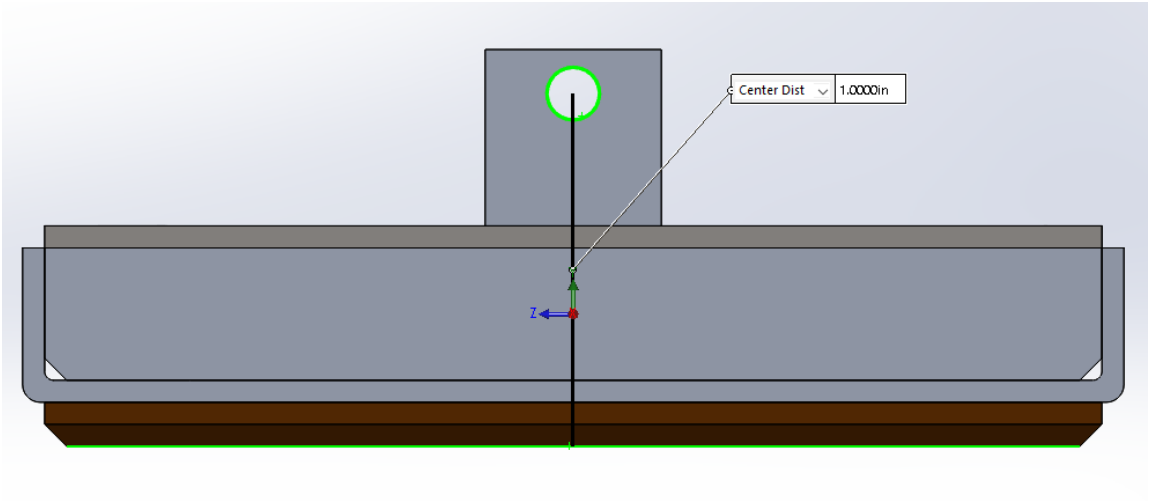

Figure 24: Right View of Assembly Shown in Figure 19 with Pivot Point Height Label

From Figure 24, SolidWorks clearly verifies that the pivot point height, located one inch above the bottom of the tribometer, is well below the calculated maximum height of one and one half inches. The half inch of leeway allows room for structural modification of these parts in future designs, if desired.

All metal components, aside from screws and any other hardware ordered from a vendor, are made from aluminum, with the exception of the beam. The beam is made of 304 stainless steel instead of aluminum to provide higher yield strength, infinite fatigue life, and resistance to corrosion. If aluminum were used for the beam material, plastic deformation may occur if loaded more than fifty pounds of force in the horizontal and vertical directions simultaneously. Using steel, however, the yield strength will be high enough to prevent plastic deformation from occurring when exposed to maximum loads based on Figure 25, which shows results from a static finite element analysis in SolidWorks.

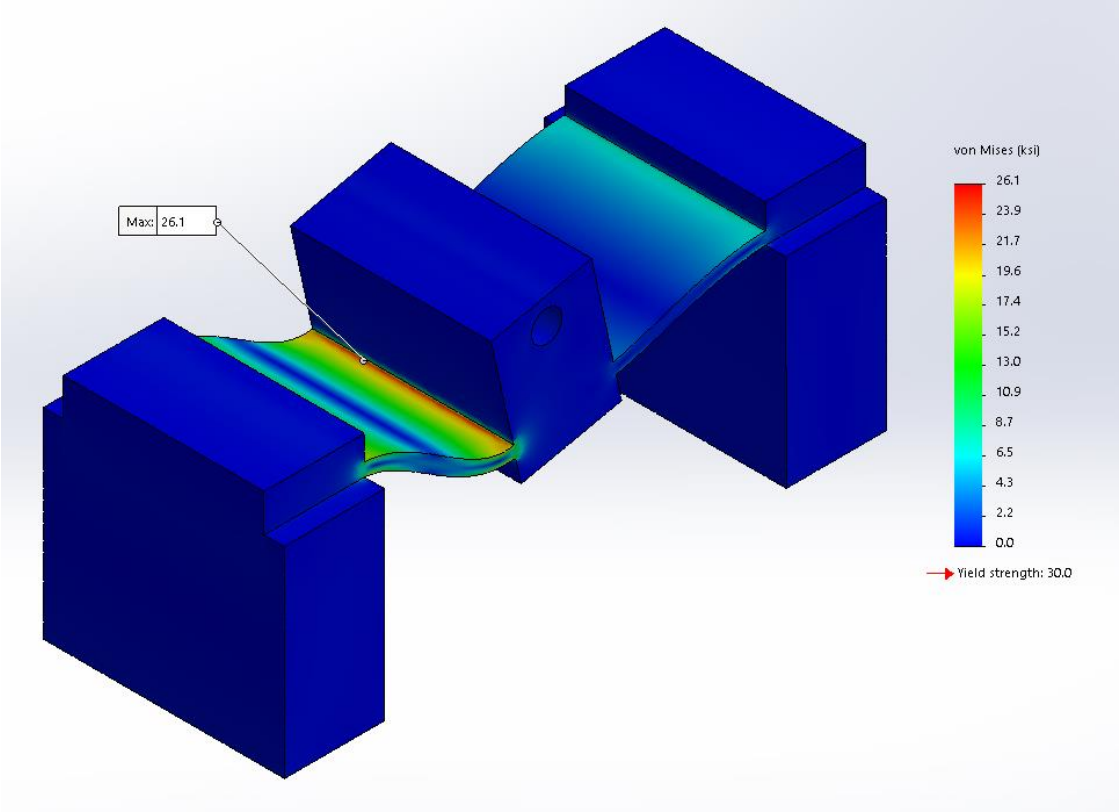

Figure 25: Stress Plot Generated from Static Study for Stainless Steel Beam Setup

The largest stress in the beam is $\sigma_{max} = 26.1\ ksi$, and the yield strength is $\sigma_y = 30\ ksi$. Using the factor of safety (FOS) formula

$$N = \frac{\sigma_{max}}{\sigma_y},$$

where $N = FOS$, the FOS is determined to be $N = 1.1$. Regarding strain output, the formula

$$\epsilon = \frac{E}{\sigma},$$

where $E = 27500\ ksi$ and $\sigma = \sigma_{max} = 26.1\ ksi$, the strain readings from the gauge located on the leading part of the beam are anticipated to be around $\epsilon = 950\ \mu in/in$.

Fatigue life is not an important quality in this stage of design, but the potentially infinite fatigue life could serve well for applications where the tribometer would be cyclically loaded frequently over a long period time. Such applications could include testing walkway material as it is manufactured and being moved along a conveyor belt, testing a certain percentage of product for quality control. This idea will be discussed more extensively in Chapter 5. The corrosion resistance characteristic of stainless steel was not a critical factor in the choice of material, but if testing is done on wet surfaces or in relatively harsh environments, the beam would be less likely to corrode.

2.4 Redesign of Electronics Enclosure and Handle

2.4.1 Issues with Prototype

The handle for Stauffer's DBFP was not ergonomically designed, nor was it aesthetically appealing. In his recommendations, Stauffer suggested a handle that would contain the wiring and battery and make the design look less busy, as shown in Figure 13. Among the problems with Stauffer's recommendation, the handle is still not comfortable to hold and use, and the case is printed, which is not cheap from a manufacturing standpoint. Rather than modifying this design, an entirely new design was proposed.

2.4.2 New Designs

During the ideation stage of redesign, the first decision was to look for a handle available for purchase. This way, an ergonomic handle can be incorporated with little effort focused on

ergonomic research and design, which can be extensive. The next thought was looking for handles on products that are used on flooring, which led to looking at handles for small vacuums. While using a small vacuum, the user is positioned in a way that mimics the intended posture of someone using the tribometer. However, no handles for small vacuums are available for separate purchase, and buying an entire vacuum just to dismantle it for the handle is too expensive and wasteful.

Firearm handles were the most abundant variety of options to investigate. With some research, the Magpul MOE Pistol Grip, shown in Figure 26, was determined to be a viable candidate for its ergonomic contour, light weight, and easy-access compartment that could serve as housing for the battery.

Figure 26: Magpul MOE Pistol Grip [13]

Because the pistol grip alone does not have enough space to house all of the electronics, an additional enclosure had to be found. In looking for regular electronics boxes, an enclosure with

a compact, yet large enough design was discovered. This enclosure is shown in Figure 27 and is manufactured by Polycase.

Figure 27: Polycase Potting Box Enclosure and Lid

The electronics anticipated to be used are one 9V battery, a microcomputer, display, and a circuit board containing a few electronic components, so a large volume is not needed for housing. To interface the case and handle, a component needs to be fabricated to be able to mate the materials, and the case must to be modified. To achieve this assembly, a wedge is proposed to serve as the site for attachment of the grip, as well as an extension from the electronics enclosure.

Before explaining the design of the wedge, the attachment process for the grip has to be understood. The grip is designed for an AR-15 rifle and has a simple design for replacing handles. To attach a grip to the rifle, the inside compartment is opened and a single screw is used to lock the grip to the rifle by threading it into a receiver on the rifle. A visual aid is shown in Figure 28, displaying a CAD model of the grip and screw used to connect the grip to the rifle.

Figure 28: Cross Section of How Grip Connects to Rifle

In designing the wedge, it was determined that it must structurally connect the grip and case, and also connect the compartments inside the grip to the electronics enclosure. This will allow a 9V battery to be carried inside the grip with wires connecting to the electronics enclosure. The proposed wedge design is shown in Figure 29, and each hole seen on the front face is cut through to the rear side of the wedge.

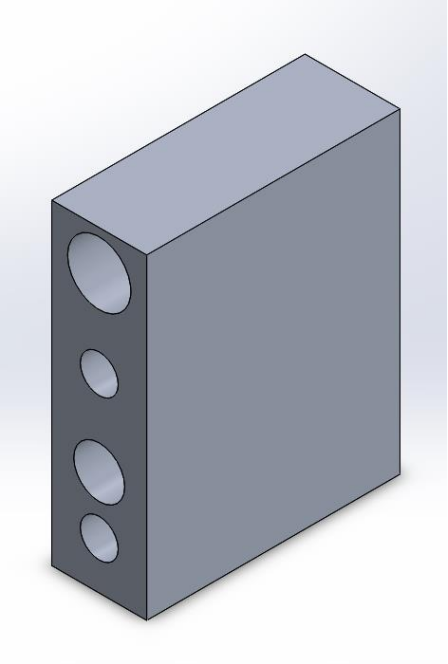

Figure 29: Isometric View of Wedge

The two small holes will be threaded and allow screws to connect the case to the wedge, while the larger, lower hole will connect the grip to the wedge. The uppermost hole serves as the contact between the electronics enclosure and compartment in the grip and will allow wires to pass through the wedge and connect a 9V battery in the grip to the electronics. By drilling some holes out of the case, connection can be made.

The last issue regarding the handle and case is connecting them to the pivot block. To achieve this, arms were made to connect the pivot block to the bottom of the case. This design can be seen in Figure 30. Note that the large hole cut through the arm from the right face is where the bearing fits, and the holes on the top face of the arm are for screws to lock the arm to the case.

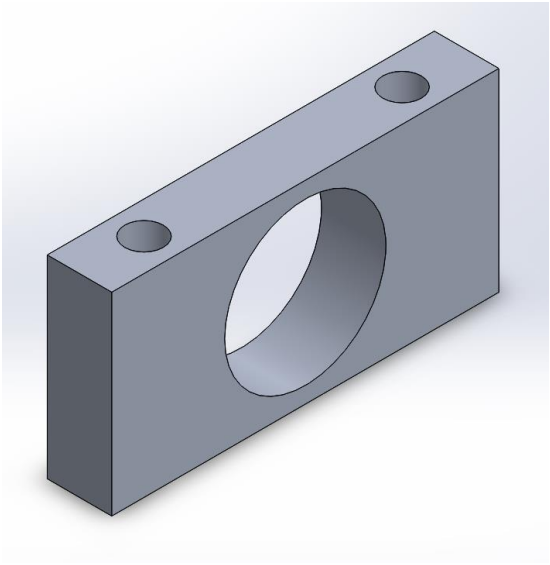

Figure 30: One of Two Arms that Connect the Electronics Enclosure to the Base

Figure 31 shows the preliminary assembly of the upper part of the tribometer. The lid is omitted from the illustration to put the volume available for electronics in perspective.

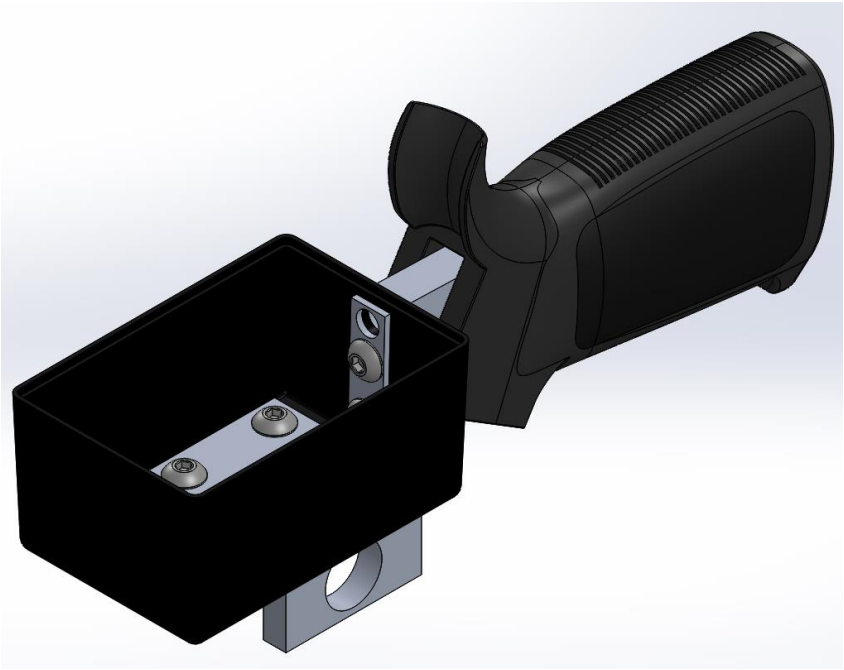

Figure 31: Preliminary Assembly of Electronics Enclosure (Lid Excluded)

2.5 Electronics

2.5.1 Strain Gauges

The DBFP has four gages with the configuration as shown in Figure 32. This Wheatstone bridge strain gauge has four gauges that each measure strain along the length of the bridge.

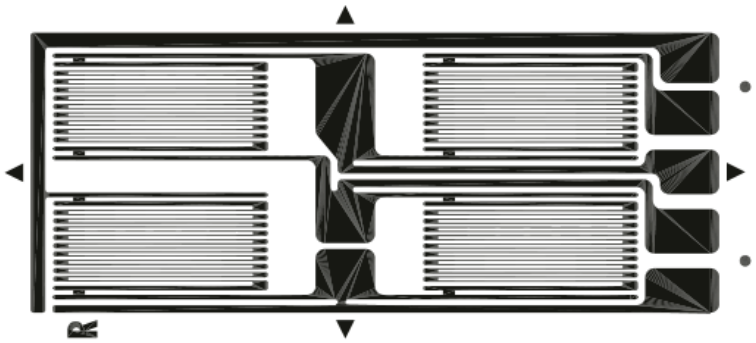

Figure 32: Full Bridge Strain Gauge Designed for Small, Double-Bending Beam [14]

While this choice of gauge is able to function well enough for a tribometer that is validated through an ANSI standard test and compared to another tribometer, a minor enhancement that can be made to eliminate some error is incorporating strain from thermal expansion. While its intended purpose is for measuring strain on transducers, temperature compensation can be incorporated using the strain gauge in Figure 33, which has two gauges measuring strain along the length of the beam and two other gauges providing thermal compensation.

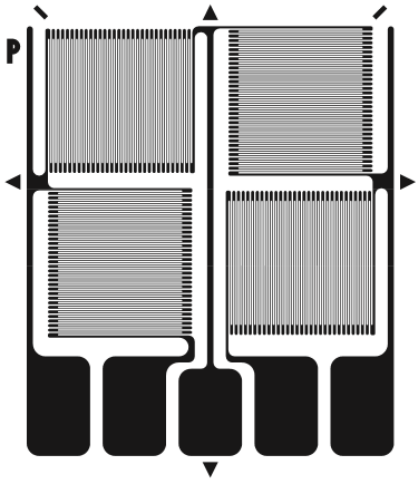

Figure 33: Full Bridge Strain Gauge for Single Surface Gauging of Transducers [14]

The original choice in strain gauge may give a more precise output of the strain measurement with two gauges measuring strain in the same locations; however, the temperature compensation allows the device to be used under a wider range of temperatures, without the loss of accuracy from measuring thermal expansion along the length of the beam during testing.

This minor change in choice of strain gauges does not have a large impact on the refinement of the device because the microprocessor program Stauffer developed involves zeroing the gauge readings immediately before testing, effectively incorporating thermal expansion of the beams. The new gauge design simply ensures any thermal expansion that may occur after zeroing gauge readings is incorporated, which should be nearly negligible. This minor refinement may benefit future designs in terms of simplifying code.

2.5.2 Microprocessor

The microprocessor used by Stauffer was the Basic Stamp II [7]. Simply put, technology has come a long way since the design of the DBFP prototype. The Basic Stamp II can only read digital inputs, which required the use of an A/D converter prior to sending the signal from the amplifier to the microprocessor. Today, microprocessors are advanced enough to read analog signals, allowing for simplification of the circuit. Figure 34 shows the simplified circuit schematic, which eliminates the two A/D converters and two Wheatstone bridges (refer to Section 2.3 for reasons bridges were eliminated). For better comprehension of the simplification, refer back to Figure 12 to see the original circuit schematic.

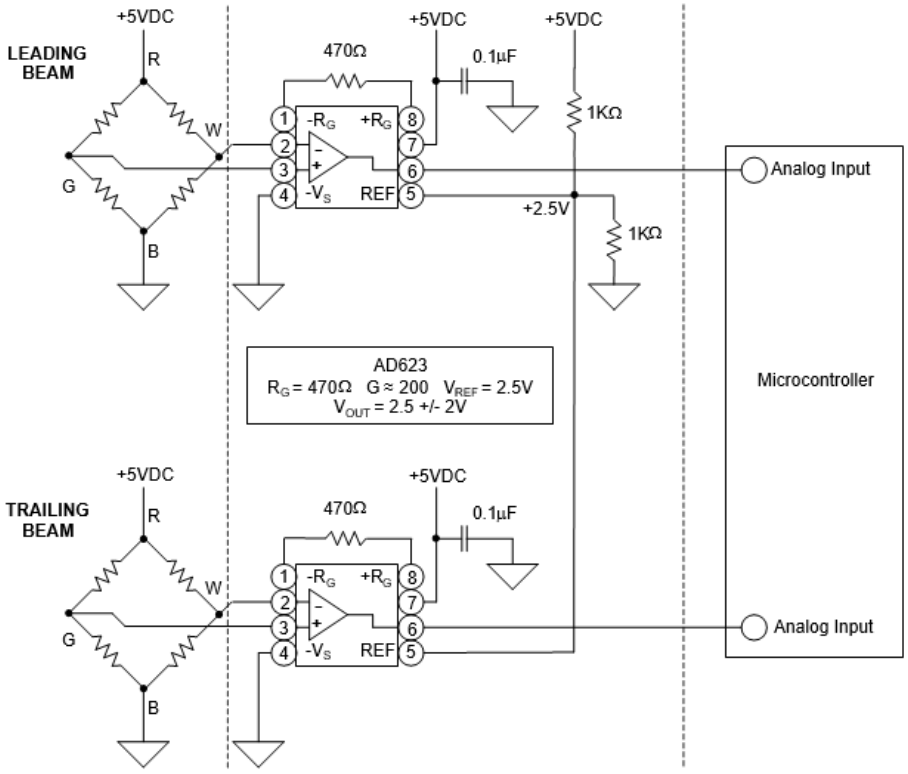

Figure 34: Simplified Circuit Schematic

Lastly, the choice of a new microprocessor comes down to interface and aesthetic appeal. For these reasons, a SparkFun USB Programmer and MicroView with an organic light emitting diode display (OLED) are recommended. The SparkFun USB Programmer board can be programmed using open-source Arduino software that can be uploaded onto the MicroView display. The SparkFun MicroView also contains an Arduino library, allowing for ease of compatibility with programming. Programming the new tribometer was not completed due to timing issues pertaining to machining the parts discussed in Sections 2.2 through 2.4. Elaboration on this shortfall, along with recommendations for avoiding such errors for future refinement on the tribometer design, are discussed in detail in Chapter 5.

Chapter 3

Refined Handheld Tribometer Assembly

3.1 Hardware

In assembling the tribometer, the Neolite, or any other desired testing material, must be attached to the shoe with an adhesive. This simple process involves coating the area the Neolite is intended to cover (entire bottom of shoe) with Superglue, pressing the Neolite pad into the shoe, maintaining pressure for a few minutes, and then letting the glue cure over a day. These are generalized instructions, and the instructions that come with any other specific glue should be followed. Once curing is finished, any glue that seeped out of the gap between the components can be removed with a scalpel and/or sand paper to give the tribometer a cleaner appearance.

When the shoe and Neolite are attached, the shoe can be slid into the mount until the holes on the front and rear faces of both pieces are concentric and the right and left faces of both components are coplanar. When in position, 10-24 x 3/8 inch screws can be threaded into the four holes that connect the shoe and mount, shown in Figure 35.

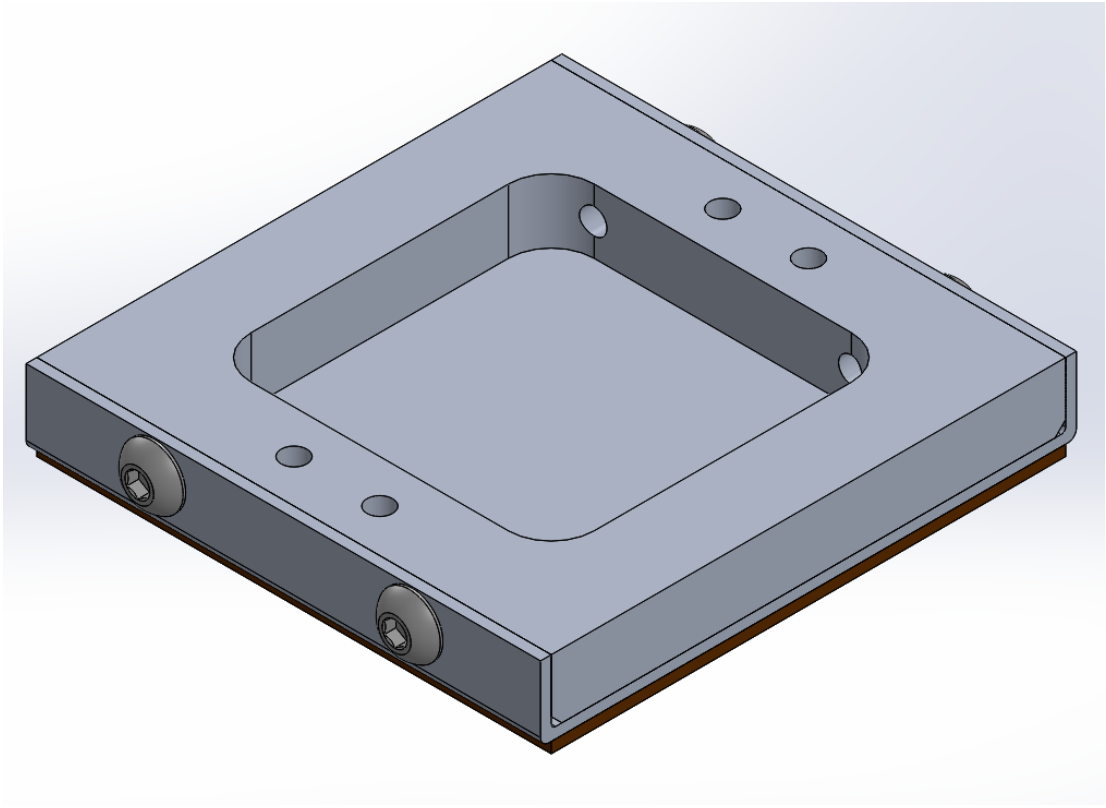

Figure 35: SolidWorks Subassembly of Neolite, Shoe, and Mount

The next set of components to be assembled is comprised of the beam and pivot block. Before describing the assembly, it is important to note that any screws used to fix the beam or any other structures susceptible to loading can cause stress concentrations where the screw is holding fixtures in place. For this reason, customized washers were developed to distribute the pressure from the screws, which is most important for uniformity of stress along the beam. Moving forward, the beam is connected to the pivot block using two 10-24 x 3/8 inch screws that are threaded into the pivot block and hold the beam, washer, and pivot block together. The subassembly should resemble the CAD model in Figure 36.

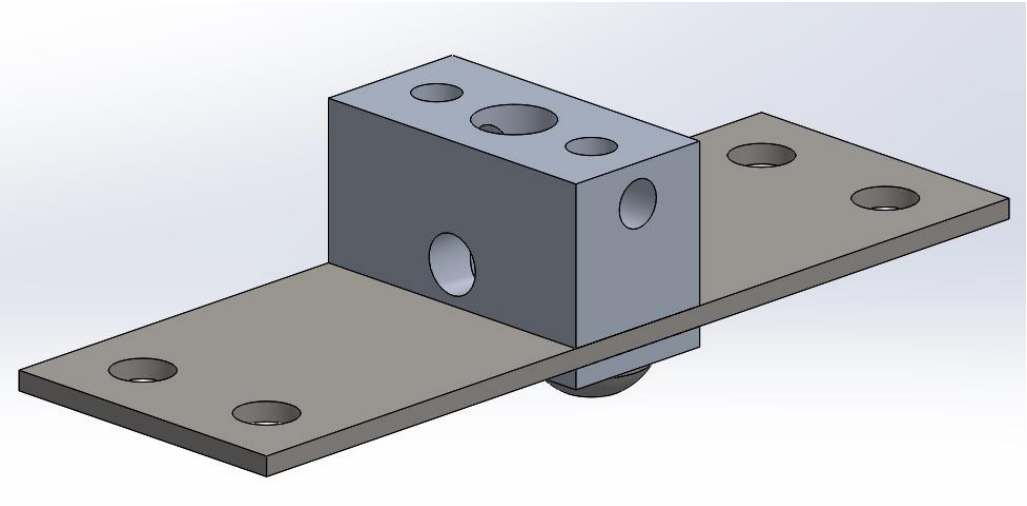

Figure 36: SolidWorks Subassembly of Pivot Block and Beam

The next simple subassembly is made up of only the arms and the bearings. The arms will hold the bearings in place with a light press fit, so the bearings must be inserted using a press to push them into place. Two subassemblies should look like the image in Figure 37. The left faces of the bearing and arm are coplanar.

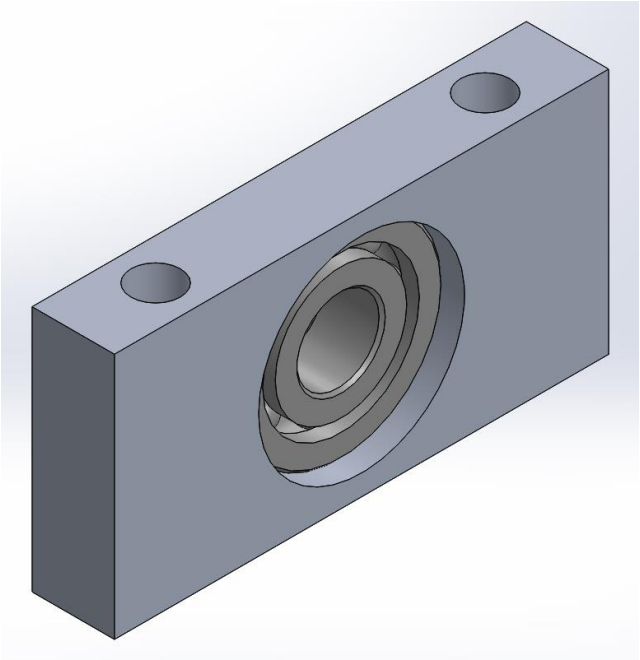

Figure 37: SolidWorks Subassembly of Arm and Bearing

The subassembly connecting the electronics enclosure is the last of the subassemblies before combing all of them into the final tribometer. The components making up the electronics enclosure are the Polycase enclosure, grip with screw (1/4-20 x 1 inch included in Magpul MOE Pistol Grip), wedge, two customized washers, and six 10-24 x 1/2 inch screws. First, the wedge is connected to the grip using the 1/4-20 thread screw. Next, two 10-24 x 1/2 inch screws are placed through the case and washer where the wedge will connect. The screws are threaded into the wedge, fixing the case, washer, wedge, and grip together. Lastly, the other washer is placed over the holes in the bottom of the case and the four remaining screws are placed in the holes to keep the washer from moving. The screws are not threaded into anything at this stage of assembly, so the screws and washer are free to move in the vertical direction. The subassembly should look like the image displayed in Figure 38.

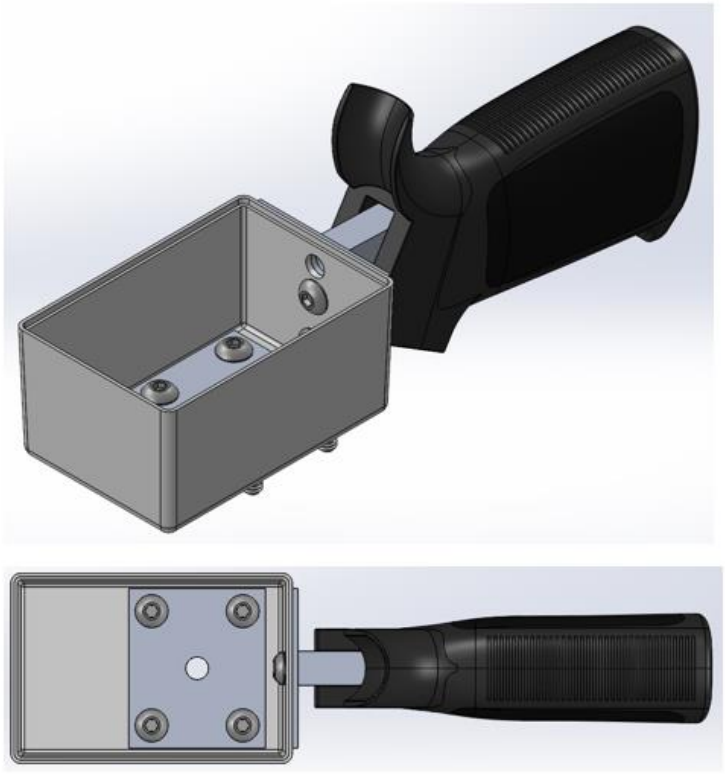

Figure 38: SolidWorks Subassembly of Case, Grip, and Wedge

The subassemblies comprised of the grip, wedge, and case are then combined with the two arms housing the bearings by threading the loose screws at the base of the case into the arms. The sides of the arms that are flush with the bearings face inward. This assembly is called the handle, shown in Figure 39.

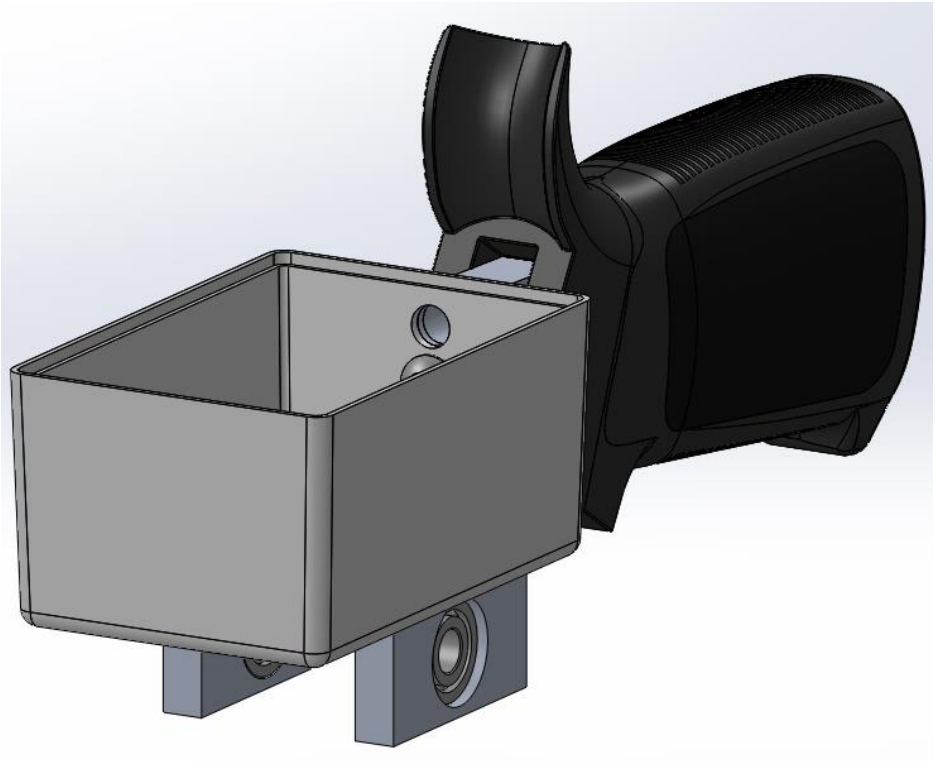

Figure 39: SolidWorks Assembly of Tribometer Handle

The remaining subassemblies make up the base of the tribometer. Mating the mount to the beam requires four 10-24 x 3/8 inch screws and two more customized washers. The two washers are placed over the two ends of the beams and the screws are threaded into the mount. The base should look like Figure 40.

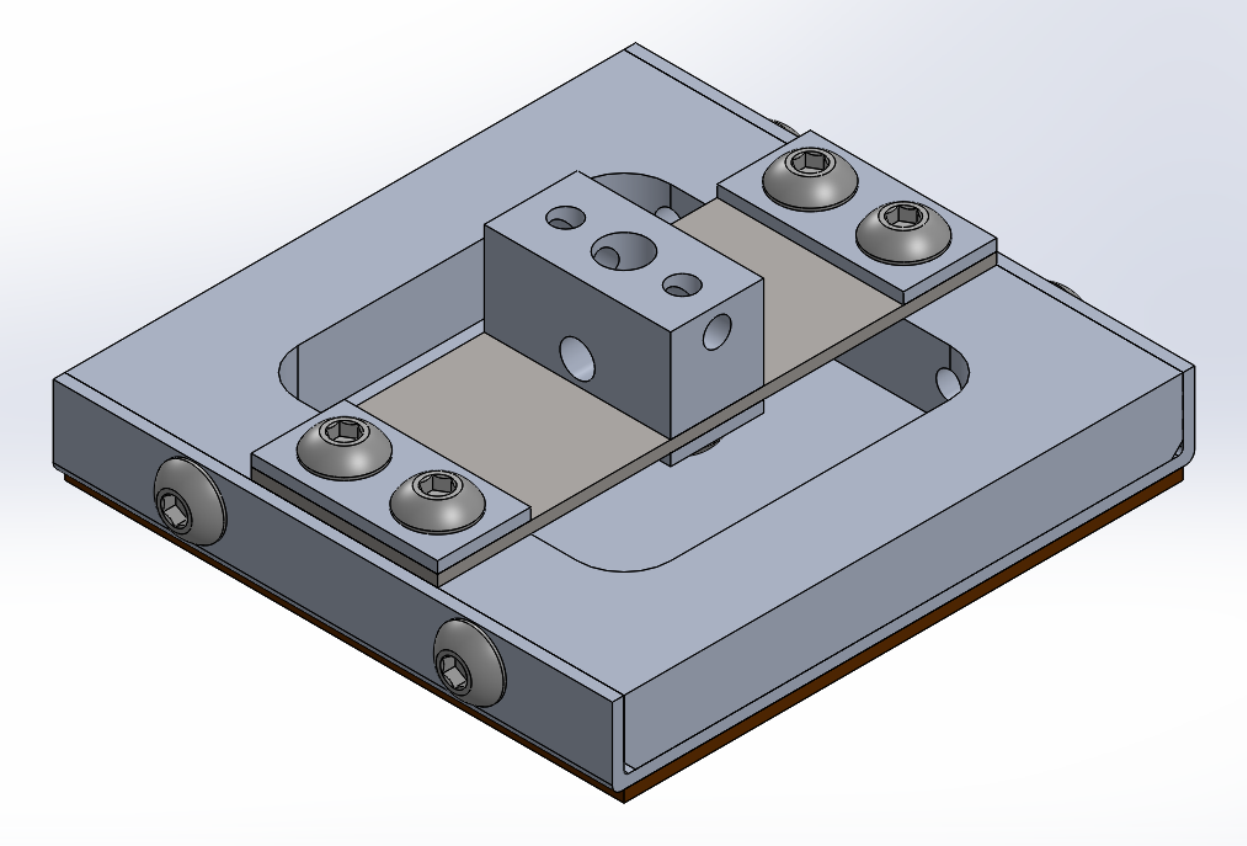

Figure 40: SolidWorks Assembly of Tribometer Base

Lastly, the handle and base are combined using the shoulder bolts. The handle is placed over the base so the bearings are concentric with the holes on the right and left sides of the pivot block. The shoulder bolts are then threaded into the sides of the pivot block, fixing the handle and base together to form the tribometer, shown in SolidWorks and physically in Figure 41 and Figure 42, respectively. Top, front, and right views of actual hardware can also be seen in Figure 43, Figure 44, and Figure 45.

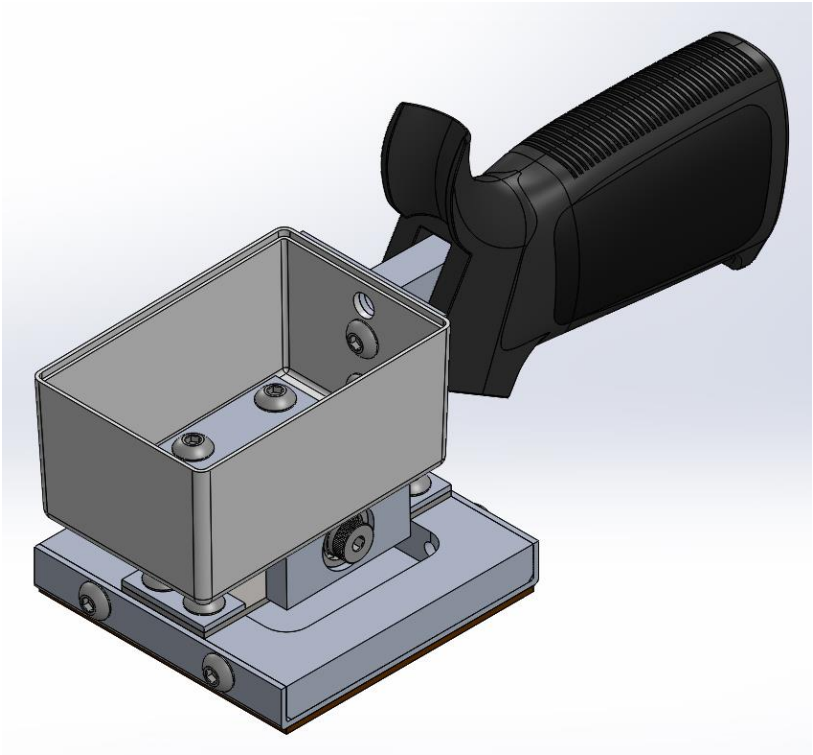

Figure 41: SolidWorks Assembly of Tribometer (No Electronics)

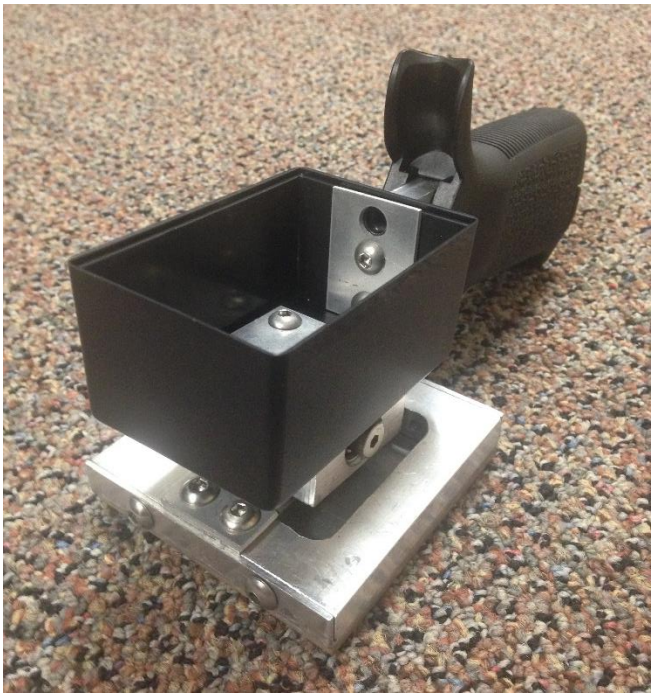

Figure 42: Isometric View of Physical Assembly

Figure 43: Top View of Physical Assembly

Figure 44: Front View of Physical Assembly

Figure 45: Right View of Physical Assembly

Some features not visible or noted in Chapter 2 are apparent now, such as the hole in the center of the case to allow the wires attached to the strain gauges to enter the electronics enclosure from the pivot block. A feature that is difficult to see, but essential to performance, is the chamfers along the leading and trailing edges the Neolite pad. The chamfers are made using sand paper and ensure the coupon does not catch or trip over any abnormities in the topography of the test specimen and report erroneous results.

Drawings developed in SolidWorks containing specific dimensions and information for all fabricated components are located in Appendix A.

3.2 Electronics

Before assembling the hardware, the strain gauges must be glued to the beam and tested to verify a signal is being sent from the gauges when strained. There are multiple steps in assembling gauges to material, with some steps varying depending on the material being tested. In short, the beam must be sanded with course sand paper, then wetted and sanded with fine sand paper. Using gauze, the residue left behind from the wet sanding must be wiped away in one direction, the surface rinsed with alcohol, re-wiped with gauze, and repeated until the gauze shows no residue. The area where the strain gauge is to be attached has to be marked so gauges can be aligned as close to the same direction as the direction of strain they are intended to measure. Using Superglue, the gauges can be attached with pressure and a bond accelerator if desired. The detail in this summary of gauge assembly is generalized and should serve only to help conceptualize the process. For installing strain gauges, reference a manual, such as Omega's User Guide for SG401 and SG496 Rapid Cure Strain Gauge Adhesives, for more detailed instructions [15].

Upon installing one of the gauges, a multimeter was used to confirm that the gauge was intact by measuring resistances across parts of the bridge. However, after soldering jumpers and wires to the beam, a signal was unable to be read. This is likely due to poor soldering skills and, more specifically, a buildup of rosin on the pads. Figure 46 and Figure 47 display the attempt at soldering wires to the gauge. Upon careful inspection, one can see droplets of hardened resin on the gauge itself and on parts of the beam, indicting enough rosin may have accumulated on the solder pads to interrupt signal conductivity.

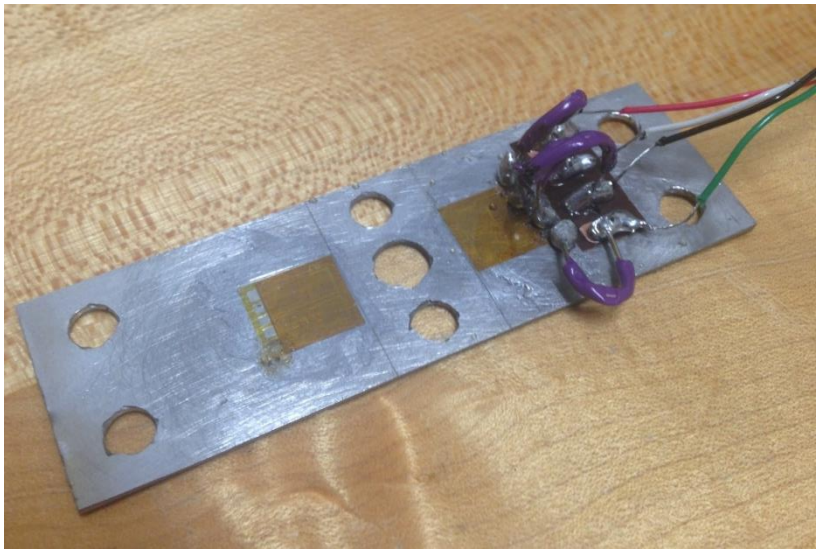

Figure 46: Beam with Two Full Bridges Installed and an Unsuccessful Soldering Attempt

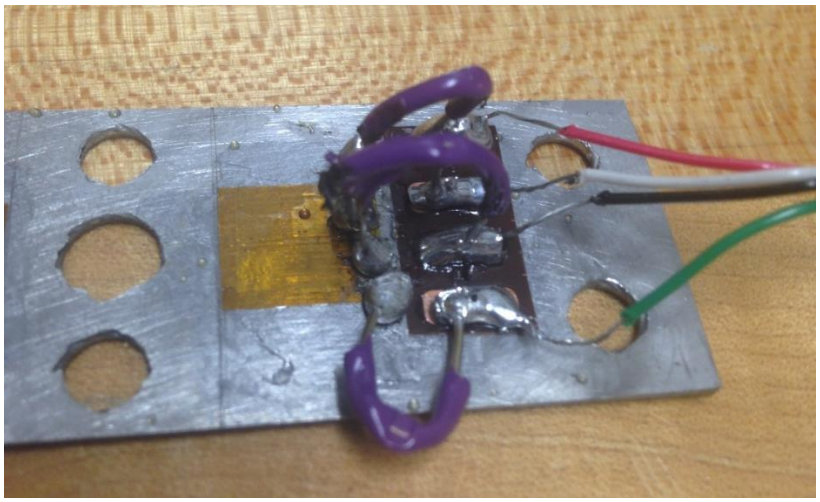

Figure 47: Close-up of Gauge with Solder Issues that Highlights Evidence of Error

Along with the rosin issue, rather large globules of solder were left on the gauge and solder pads as well. Visual inspection indicated there were no short circuits bridging two or more pads together with one oversized drop of solder, but the layer of rosin between the solder and solder pads prevented troubleshooting using the multimeter.

If resistances were able to be read on the wires, indicating the soldering successfully connected the gauge circuit and wires, the setup in Figure 48 would allow for reading outputs and translating them to strain measurements. The device the gauge is wired to is a strain indicator.

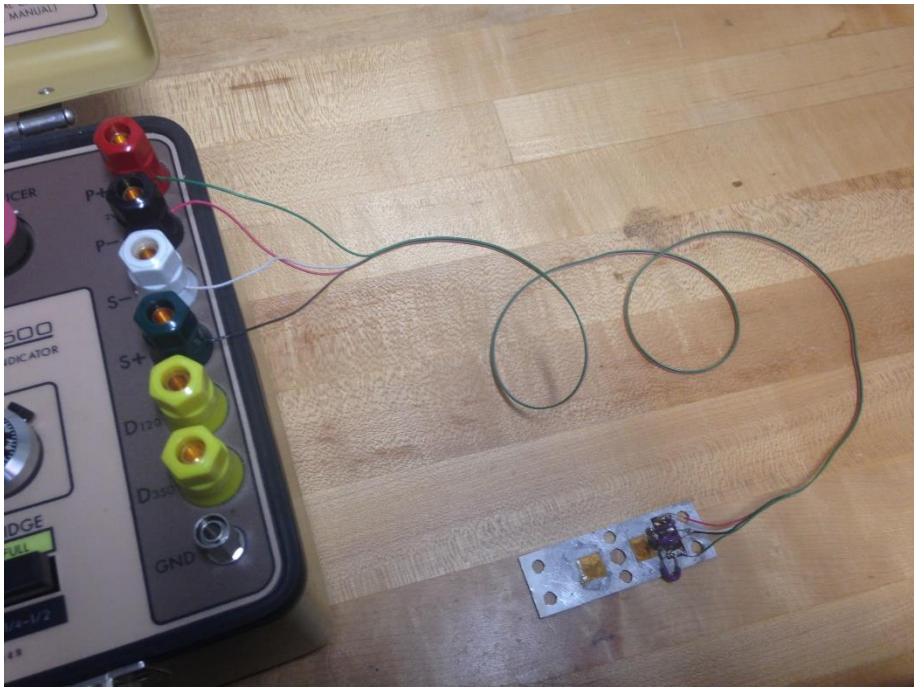

Figure 48: Setup of Bridge Wired to Strain Indictor to Display Strain Readings

The takeaways from this failure are discussed in detail in Chapter 5, along with advice on how to avoid repeating such failures when refining the design in future work. Because a signal was not obtained from the gauges during beam deflection, data processing using a microcontroller was not pursued in this thesis.

Chapter 4

Standards for Testing

4.1 American National Standards Institute Terminology

Among the most pertinent ANSI standards for testing walkway surfaces are ANSI/NFSI-B101.3 and NFSI-101C. B101.3 refers to hard-surface material, such as tiles, while 101C refers to floor mat backing [16], [17]. Each standard describes detailed cleaning and testing procedures for its designated walkway specimen, carefully outlining how many times a procedure has to be done, what constitutes valid data, and how to interpret results. B101.3 describes a more rigorous testing procedure than that described in 101C, but the simplified procedure in 101C still strongly resembles the procedure in B101.3.

4.2 Test Procedures

ANSI sets standards for slip-resistance and minimum COF available for walkway surfaces. Similarly, ANSI sets standards for testing walkway surfaces and, therefore, plays a role in the design and function of the devices used to measure these surfaces. Among the most important features of a tribometer is repeatability, and ANSI has a specific procedure for testing dry and wet surfaces.

The test procedure that is specific to every individual slip-resistance test is stated in ANSI-B101.3. The first step of the procedure is to analyze the uninstalled flooring samples and ensure they meet the manufacturer's specifications to +/- 5% [16]. The samples to be tested are selected

at random from a batch of typical samples and then cleaned with a mild detergent, distilled water, and an untreated paper towel [16]. For DCOF measurements, the surface should be wetted using a surfactant solution of sodium lauryl sulfate in distilled water [16]. When the specimen preparation is completed, the testing can commence according to the tribometer manufacturer's operating instructions [16].

The testing has to be done with careful attention focused on the direction in which the testing is conducted. With the cleaned sample placed in a way that no shifting will occur during testing, testing should be done in one direction five times, with the result from each test recorded [16]. After data has been collected in one direction, the process is repeated three more times, each at a 90-degree clockwise rotation from the previous test direction, resulting in twenty slip-resistance measurements for the specimen [16]. After one sample has been tested, the entire process, starting with cleaning and ending with the twentieth measurement, is to be repeated for three more separate samples [16].

Upon conclusion of the physical tests, data analysis is performed to validate the accuracy and precision of the tribometer readings. The average and sample standard deviation of all sixty readings are calculated, and the sample standard deviation is divided by the average to obtain the coefficient of variation (COV) [16]. The COV simply represents the percent value of standard deviation and is not to exceed 0.10 [16]. If the COV does exceed 0.10, the data is invalid and the testing procedure and/or tribometer must be re-tested or corrected [16]. For data sets that are valid, the DCOF are calculated (if not already part of the output of the tribometer) and evaluated

to be deemed highly slip resistant (DCOF > 0.45), acceptably slip resistant (0.45 > DCOF > 0.30), or slightly slip resistant (DCOF < 0.30) [16].

Slip resistance testing can be done on installed flooring as well, but the process differs slightly. The first difference is that the test only needs to be conducted in two directions – the first in any direction, and the second 90 degrees clockwise to the first direction – and only three readings are taken in each direction [16]. The second difference pertains to the data analysis, in that upper and lower bounds are calculated instead of a sample standard deviation [16]. The average of the data is taken and the upper and lower bounds of +/- 10% are created [16]. If all data readings fall within the bounds, the data is valid and evaluated in the same manner for uninstalled flooring samples described above [16].

From this standard, it is clear that installed surfaces are more susceptible to misreading and erroneous conclusions than uninstalled flooring samples, with regard to slip resistance. Because of the difference in quantity of data readings, just one erroneous data point has a stronger effect on the calculated average and can invalidate an entire test for installed surface tests. On the other hand, if enough erroneous readings are taken, a valid test can assign an incorrect slip resistant evaluation to a walkway surface, potentially increasing the chance of harm for a human walking on the surface. In both testing environments, it is critical that the tribometer in use has high repeatability so that tests are valid according to ANSI standards and, therefore, reduces the likelihood of erroneous readings than can result in harm to the public.

After reviewing the detail described in B101.3, the 101C procedure for floor mat backing can be seen as much less rigorous that than in B101.3, but is restricted to testing with specific tribometer models. Like B101.3, 101C testing procedures require random samples be used, specifically three 3 x 3 inch samples, and be adhered to the shoe of the tribometer using double sided carpet tape [17]. After the first sample is taken, the second sample must be taken at a 45-degree angle from the first sample, and the third sample 90-degrees to that of the first sample [17].

The tribometer will then test the specimen on a NFSI certified test tile that has been cleaned using de-natured alcohol [17]. Once the test tile is clean, the measuring device is to test the specimen once in one direction and then record the COF that was calculated from the test [17]. This step is repeated three more times, rotated 45-degrees after each test, and the COF recorded after each test [17]. Once four measurements have been taken with the first test sample, the same four tests are to be repeated for the remaining two samples [17]. The average of each test for a sample is the COF for the specimen and is classified as demonstrating “High Traction” characteristics if the value is above 0.50 [17].

Chapter 5

Recommendations for Future Work

5.1 Problems Encountered and Lessons Learned

The most notable challenge faced in the project was learning to fabricate the customized parts. In the initial schedule, the “fabricating parts” stage was only allocated about a month, which seems to be enough time to fabricate the parts shown in Appendix A. However, no experience existed with machining before, so many errors were made, parts were cut incorrectly after hours of making them, parts would not fit together and require rework, and the learning curve was very slow because of the specific nature of machining. While the original time frame to machine parts was doubled from initial predictions to allow for a time cushion, it was not enough to compensate for the lost time. All parts are now fabricated for future testing, but if any machining has to be done, it is advised to start with simple test parts to practice as soon as possible so mistakes can be made on parts that are not meant to make up the final product.

Another time issue arose from iterating on the CAD model for too long, honing in on better and better designs. Because designing can continue for very long periods of time, a design that just sufficed should have been accepted early to allocate enough time for refinement of other systems. As a result, the structure, cost, and aesthetics of the device have improved dramatically since the DBFP design, but the new design has an entire system (electronics) barely planned and not experimentally proven to work. The only refinement with regards to the electronics systems is on paper, so future refinement of the tribometer can have a head start with designing electronics and programming for the device.

5.2 Recommendations for Next Iterations

To properly compete with other tribometers on the market, it would be wise to at least have the capabilities they have, specifically data storage and retrieval, real-time COF readings, and signals like beeping and flashing LEDs so users can tell when a battery needs replaced or system level concerns arise. Regarding the structural aspect of the design, the Polycase enclosure made of plastic requires the use of washers in order to help distribute force over an area so the enclosure does not fail during testing. This case can be replaced with a metal case that would not only better maintain the structural integrity of the tribometer, but also eliminate the need for the washers that are used to distribute the force. The alternative diecast enclosure from Polycase shown in Figure 49 was the last design choice made, but due to time constraints, the plastic enclosure was pursued.

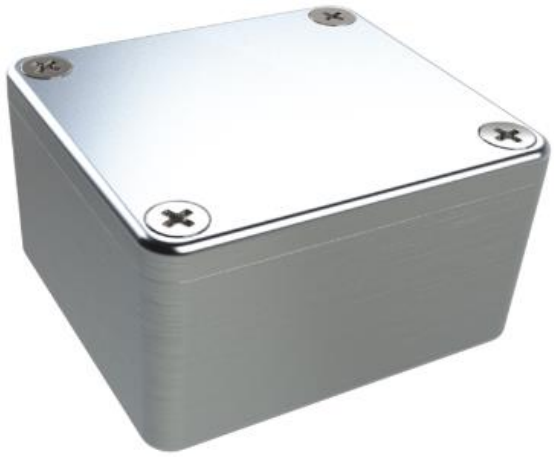

Figure 49: Polycase Diecast Aluminum Enclosures

When refinement of the current tribometer design reaches production stages, geometric dimensioning and tolerancing (GD&T) should be emphasized in the drawings for parts listed in Appendix A. As of now, the drawings suffice for individual fabrication, where researchers can look at the dimensions and determine whether under sizing or oversizing can be permitted. On a mass production scale, however, adhering to GD&T guidelines could reduce error and ambiguity in fabrication.

5.3 Design for Specific Applications

Some applications for the tribometer can be explored beyond just individual walkway surface testing and certification. One such application, briefly mentioned in Chapter 2, is quality control in walkways surface manufacturing plants. For example, a robotic device could be programmed to test one in every ten products to come out of production and record results. For such an application, fatigue analysis could be done on the beam to ensure the device would not need repaired or replaced by keeping stresses below the endurance limit for the beam. Theoretical models could be developed to find the theoretical fatigue limit, and simulations could be run using SolidWorks to verify the results.

BIBLIOGRAPHY

[1] "Nonfatal Occupational Injuries and Illnesses Requiring Days Away from Work." Internet: https://www.bls.gov/news.release/archives/osh2_11102016.pdf, Nov. 10, 2016 [Accessed Apr. 1, 2018].

[2] "2016 Survey of Occupational injuries and Illnesses." Internet: https://www.bls.gov/iif/osch0060.pdf, Nov. 9, 2017 [Accessed Apr. 1, 2018].

[3] Burns, Elizabeth. "The direct costs of fatal and non-fatal falls among older adults - United States," Journal of Safety Research, vol. 58, no. 1, p. 99-103, September 2016. [Online]. Available: ScienceDirect, http://www.sciencedirect.com. [Accessed February 20, 2017]

[4] Florence CS, Bergen G, Atherly A, Burns ER, Stevens JA, Drake C. "Medical Costs of Fatal and Nonfatal Falls in Older Adults." Journal of the American Geriatrics Society, March 2018. [Online]. Available: Wiley Online Library, https://onlinelibrary.wiley.com/doi/abs/10.1111/jgs.15304 [Accessed Apr. 1, 2018]

[5] C. M. Powers, et al. "Assessment of Walkway Tribometer Readings in Evaluating Slip Resistance: A Gait-Based Approach," Journal of Forensic Sciences, vol 52, no. 2, p. 400-405, March 2007. [Online]. Available: Wiley Online Library, http://onlinelibrary.wiley.com. [Accessed February 20, 2017].

[6] "National flooring Safety Institute." Internet: https://nfsi.org/, Oct. 24, 2017 [Accessed Apr. 1, 2018].

[7] J. Stauffer, "Validation of a Handheld Friction Tester," M.S. Thesis, Dept. Mech. Eng., The Pennsylvania State Univ., State College, PA, 2001.

[8] "Slide Measuring Instrument GMG 200." Internet: https://www.gte.de/material/BDA_GMG200_eng.pdf, June 2006 [Accessed Apr. 1, 2018].

[9] "BOT-3000E Digital Tribometer Operating Manual." Internet: http://www.reganSci.com/index_htm_files/BOT3000E%20USER%20MANUAL%20V1.50.pdf, Jan. 2018 [Accessed Apr. 1, 2018].

[10] "Gold Standard 1 Coefficient of Friction Slip Meter." Internet: http://gsslipmeter.com/, [Accessed Apr. 1, 2018].

[11] "MAD Safety Instruments." Internet: https://www.madsafetyinstruments.com/, [Accessed Apr. 1, 2018].

[12] "Kett." Internet: https://kett.com/, [Accessed Apr. 1, 2018].

[13] "Magpul." Internet: https://www.magpul.com/, [Accessed Apr. 3, 2018].

[14] "Micro-Measurement, a Vishay Precision Group Company." Internet: http://www.vishaypg.com/micro-measurements/list, [Accessed Apr. 5, 2018].

[15] "Omega User's Guide." Internet: https://www.omega.com/manuals/manualpdf/M1270.pdf, [Accessed Apr. 5, 2018].

[16] *Test Method for Measuring Wet DCOF of Common Hard-Surface Floor Materials*, ANSI/NFSI B101.3, 2012.

[17] *NFSI 101-C Test Method for Measuring Dry TCOF of Floor Mat Backing Materials*, NFSI 101-C, 2010.

APPENDIX A

SolidWorks Drawings of Fabricated Parts

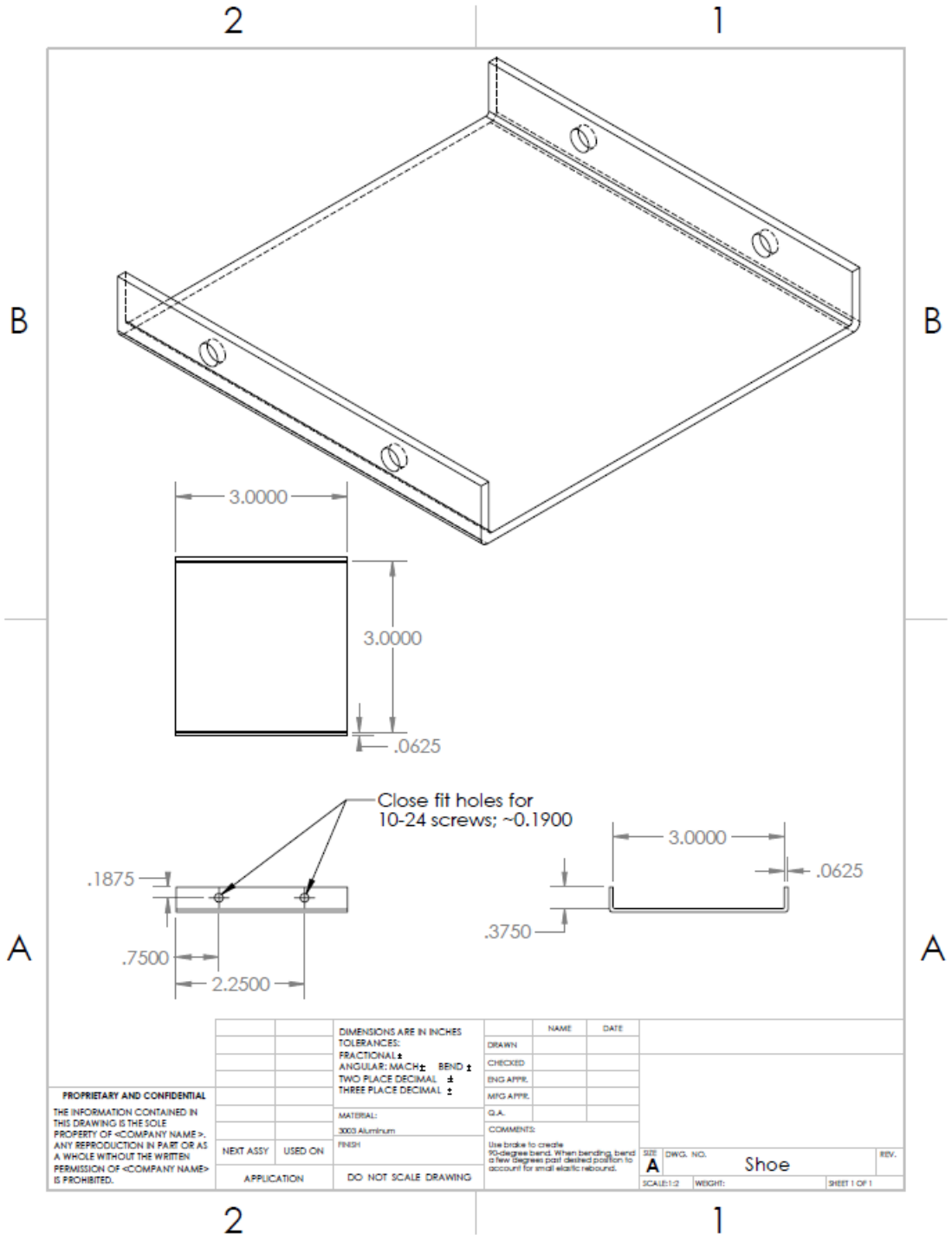

Figure 50: SolidWorks Drawing of Shoe

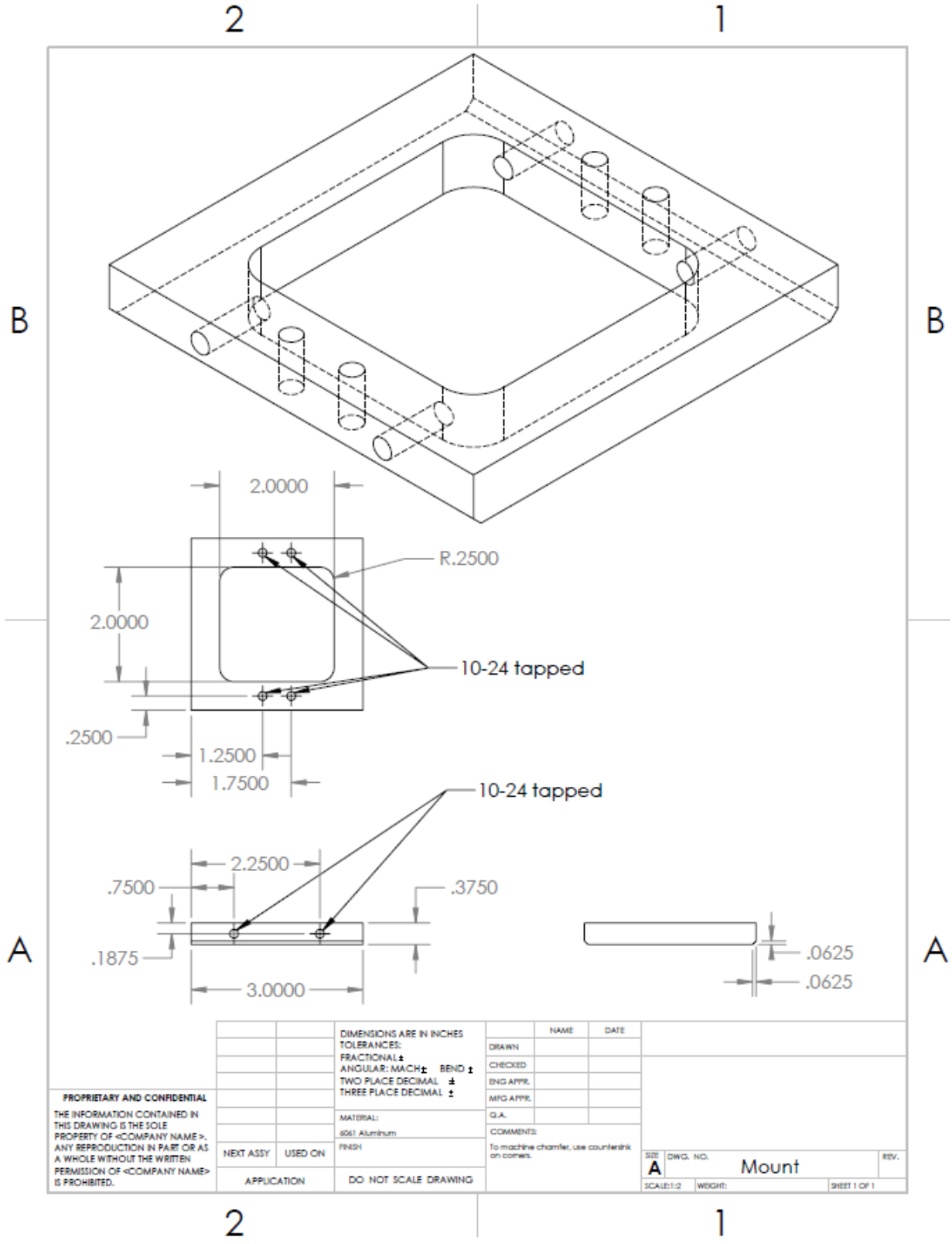

Figure 51: SolidWorks Drawing of Mount

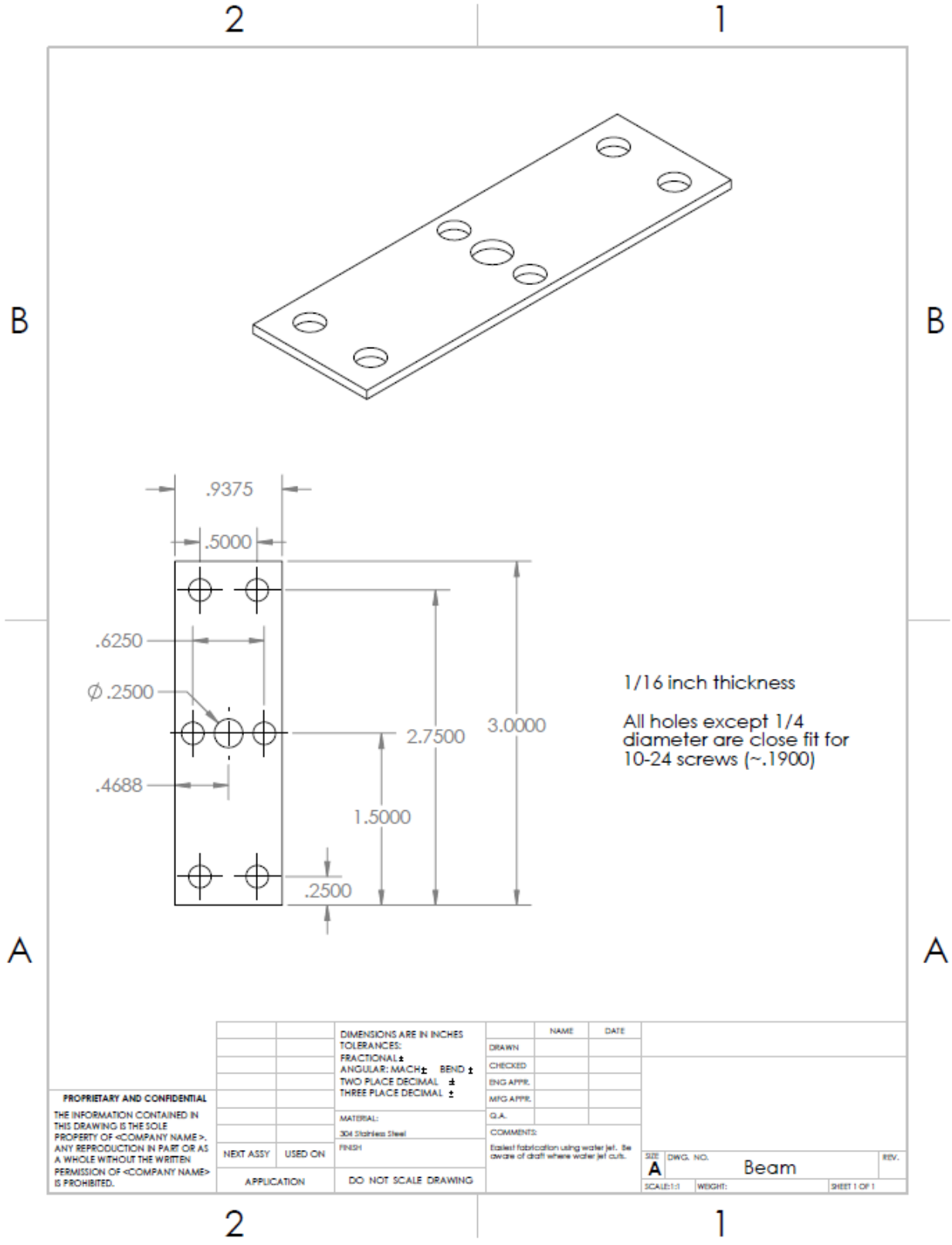

Figure 52: SolidWorks Drawing of Beam

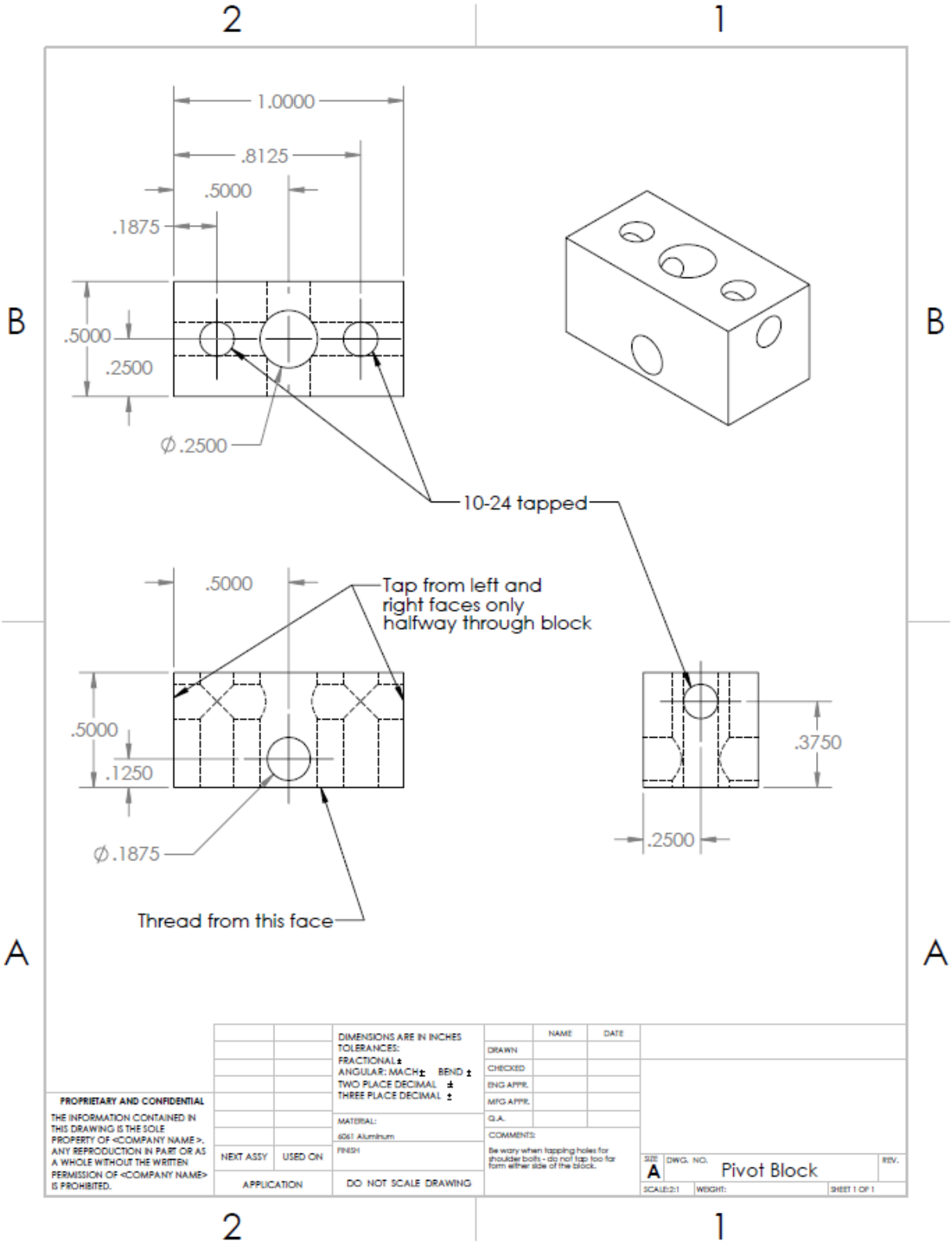

Figure 53: SolidWorks Drawing of Pivot Block

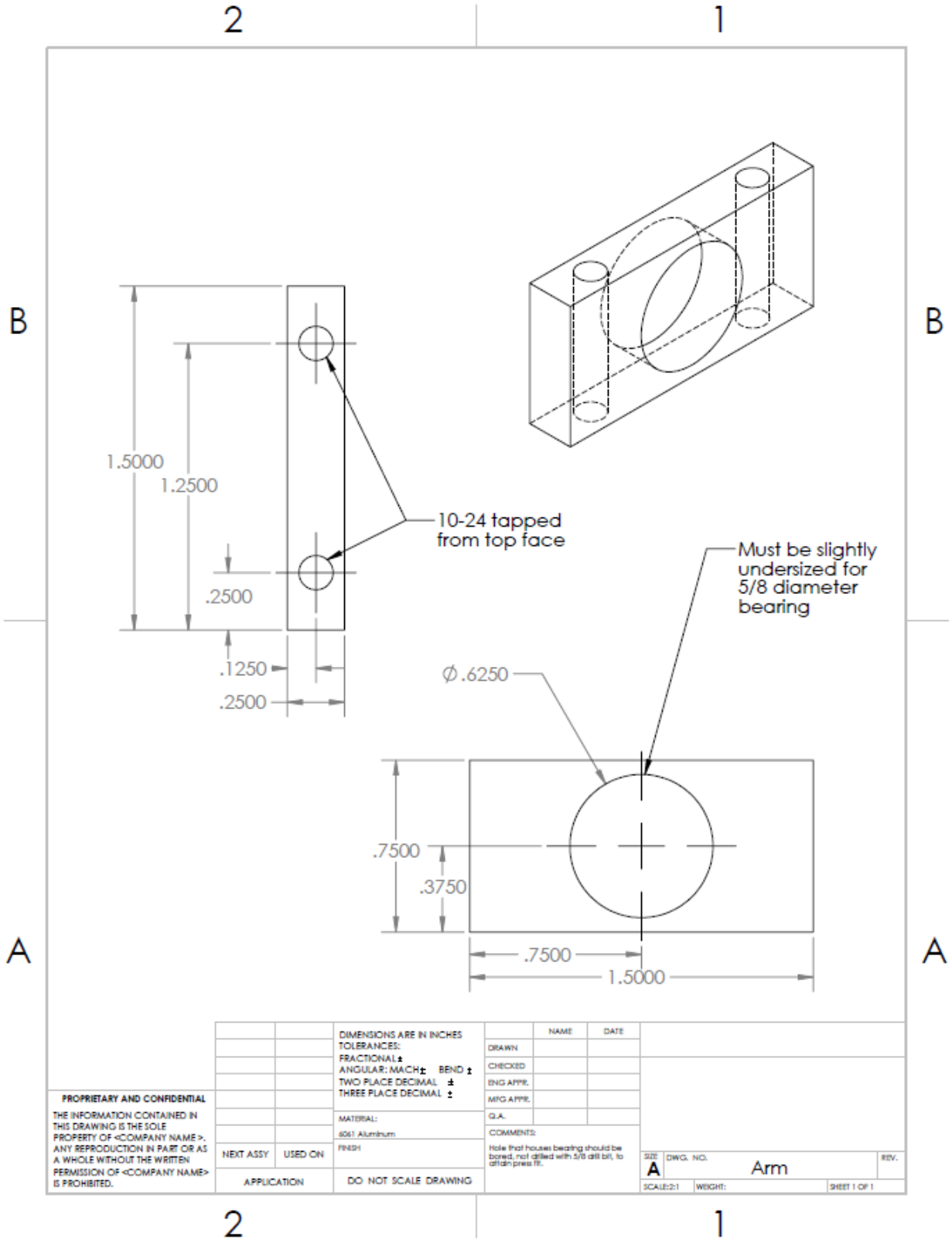

Figure 54: SolidWorks Drawing of Arm

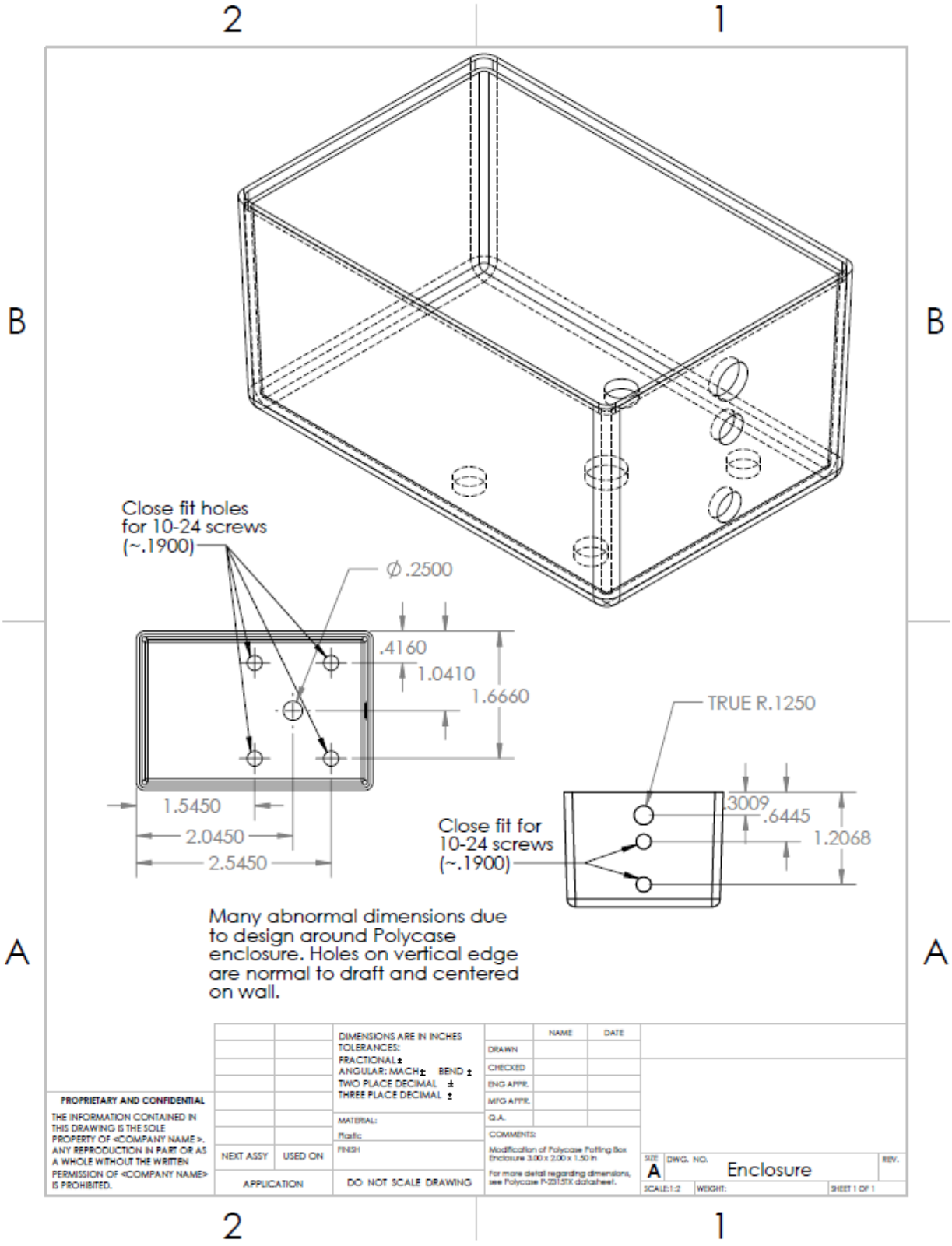

Figure 55: SolidWorks Drawing of Enclosure

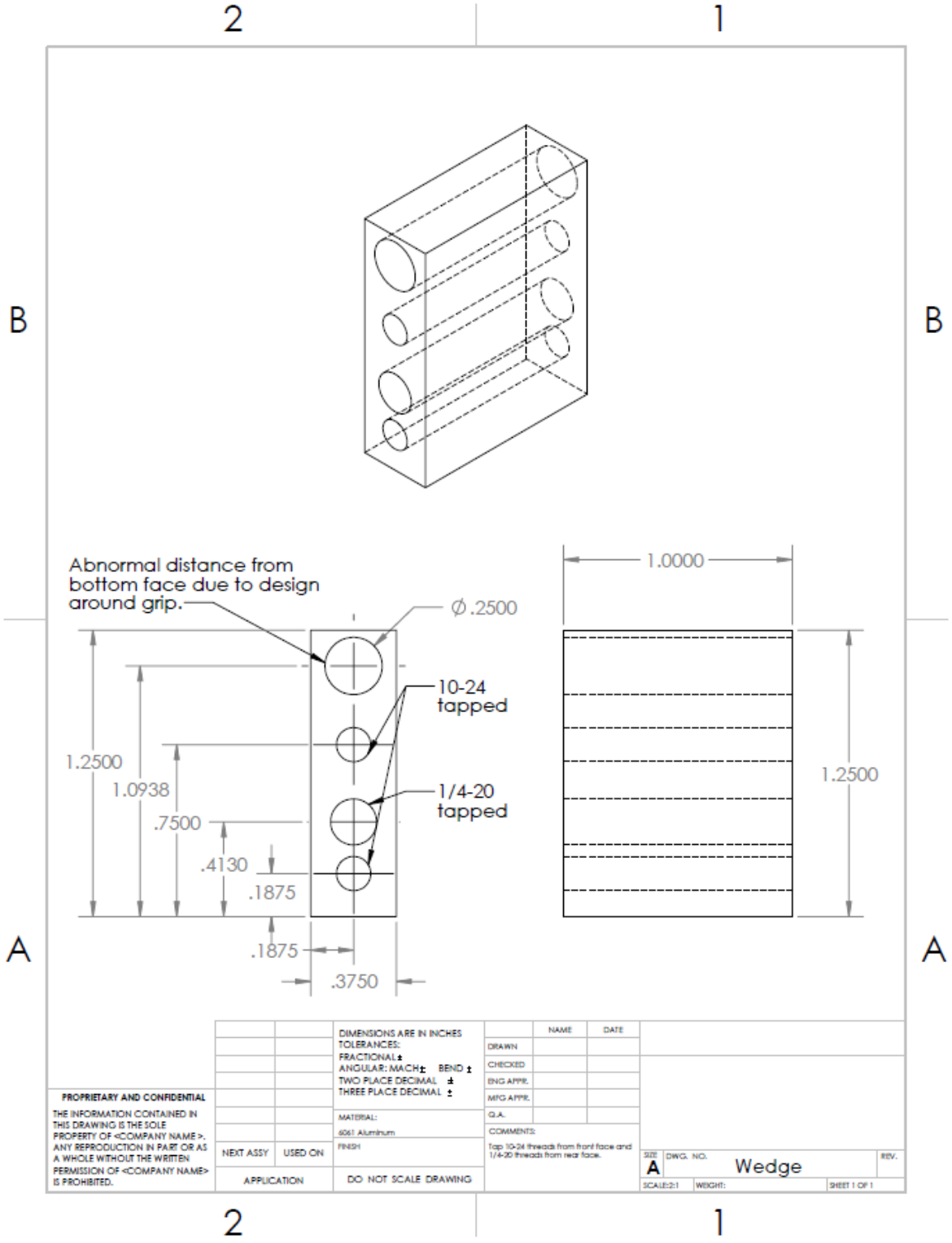

Figure 56: SolidWorks Drawing of Wedge

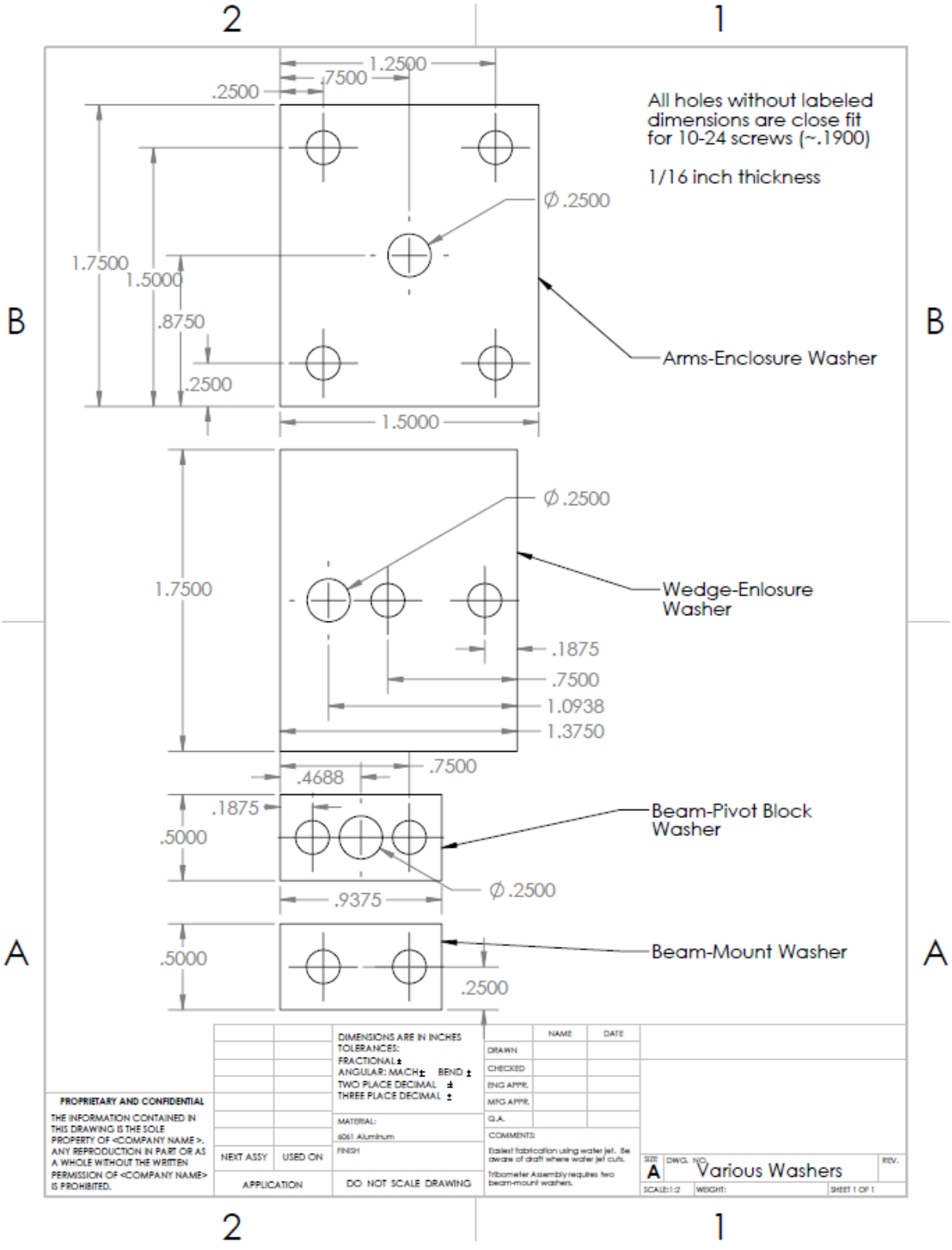

Figure 57: SolidWorks Drawing of Washers

APPENDIX B

Bill of Materials

Table 4: Bill of Materials

Part Name / Labor Expense	Part Number	Fabricated	Vendor[a]	Vendor Part Number[b]	Quantity	Unit Price ($)[c]
Neolite 6 x 6 x 1/4 inch	01		Smithers Rapra	(Custom Order)	1	245.99
Shoe	02	X	McMaster-Carr	8973K137	1	2.81*
Mount	03	X	McMaster-Carr	8975K91	1	6.41**
Beam	04	X	McMaster-Carr	8983K115	1	5.10
Washer, Beam-Mount	04-W	X	McMaster-Carr	8973K137	2	(Shoe)*
Pivot Block	05	X	McMaster-Carr	9008K81	1	1.59
Washer, Beam-Pivot Block	05-W	X	McMaster-Carr	8973K137	1	(Shoe)*
Arm	06	X	McMaster-Carr	8975K618	2	2.07
Washer, Arms-Enclosure	06-W	X	McMaster-Carr	8973K137	1	(Shoe)*
Wedge	07	X	McMaster-Carr	8975K91	1	(Mount)**
Washer, Wedge-Enclosure	07-W	X	McMaster-Carr	8973K137	1	(Shoe)*
Shoulder Bolt	08		McMaster-Carr	90298A530	2	2.35
Ball Bearing	09		McMaster-Carr	60355K503	2	5.77
Enclosure	10-E	X	Polycase	P-2315TX	1	1.54
Cover	10-C		Polycase	C-0203-N	1	0.76
Grip	11		Magpul	MAG415	1	19.95
Display	12		SparkFun	DEV-12923	1	24.95
10-24 x 3/8 inch Screw	13		McMaster-Carr	92949A240	6	6.04***
10-24 x 1/2 inch Screw	14		McMaster-Carr	92949A242	10	6.32***
Strain Gauges			Omega	SGT-3G/350-FB41	5	127.99
Water Jet Cutting			Penn State Learning Factory			100.00
					Total	**563.64**

[a]Vendors for fabricated parts are the vendors for the raw material needed to fabricate the part.
[b]Part numbers for fabricated parts refer to minimum material required to fabricate part.
[c]Cost of machined parts refers to minimum raw material required and excludes machining costs.
*Shoe and all washers can be fabricated from same sheet.
**Mount and wedge can be fabricated from same bar.
***Cost of 100 pack

ACADEMIC VITA

2189 Reservoir Heights Drive, Hanover, PA 17331 | (717) 524-6185 | nsn5035@psu.edu

Education

THE PENNSYLVANIA STATE UNIVERSITY, University Park, PA **Graduation Date:**
Penn State Schreyer Honors College **May 2018**
Bachelor of Science in Mechanical Engineering
Bachelor of Science in Nuclear Engineering
Minor in Environmental Engineering

Work Experience

Engineering Safety Analysis Intern **May 2017 - August 2017**
Exelon Generation Headquarters, Kennett Square PA

- Developed a program using Visual Basic for Applications to optimize how long control room operators need to wear a self-contained breathing apparatus after a loss-of-coolant accident
- Performed dose analysis using RADTRAD to determine exposure levels to operators in the control room after a loss-of-coolant accident and what protection measures need to be taken

HVAC Engineering Intern **May 2016 - August 2016**
Evapco World Headquarters, Taneytown MD

- Worked in R&D by operating a wind tunnel to test fan performance while manipulating variables such as tip clearance, cowl length, fan blade pitch, horsepower, and number of blades
- Acquired skills in three-phase power measurement, performance measurement, and metal working through collaboration and testing with senior engineers and technicians

Peer Tutor **January 2014 - August 2015**
The Pennsylvania State University, York PA

- Tutored in and led group study sessions for chemistry, physics, and mathematics on a weekly basis
- Strengthened abilities to convey ideas through explaining the same subjects to multiple different audiences, such as adult learners, students with disabilities, and recent high school graduates

Involvement

- Tau Beta Pi Engineering Honors Society
- Alpha Nu Sigma National Honors Society
- American Society of Mechanical Engineers
- Engineers for a Sustainable World
- Engineers Without Borders
- American Nuclear Society

Skills

- Circuit Building with Arduino Microcontrollers
- Technical Writing
- Certified SolidWorks Associate
- Metalworking and Machining
- Proficient MatLab
- Novice Visual Basic for Applications
- Novice Linux
- CRLA Advanced Level Tutor